

---

---

# **A computational fluid dynamics study to evaluate the effect of an air-cooled fuel cell stack using a turbulence inducing grid under transient operating conditions**

---

---

Masters Thesis - Thermal Energy and Process Engineering  
by Alexander Strømfeldt Lind

Aalborg University  
Department Of Energy Technology

Copyright © Aalborg University 2019

Typesetting and formatting the document was done using the  $\text{\LaTeX}$  document preparation system. For the computational fluid dynamics study, ANSYS Fluent 19.2 was used (Academic License) and CFD-Post for post-processing the data obtained. Figures, graphs and illustrations was created using Microsoft Visio 2016 and Tecplot 2011.



Institute Of Energy Technology  
Aalborg University  
<http://www.et.aau.dk>

## AALBORG UNIVERSITY

### STUDENT REPORT

**Title:**

A computational fluid dynamics study to evaluate the effect of an air-cooled fuel cell stack using a turbulence inducing grid under transient operating conditions

**Theme:**

Self-elected master's thesis

**Project Period:**

Spring semester 2019

**Project Group:**

TEPE4-1003

**Participant(s):**

Alexander Strømfeldt Lind

**Supervisor(s):**

Torsten Berning  
Chungen Yin

**Copies:** 0**Page Numbers:** 56**Date of Completion:**

May 30, 2019

**Abstract:**

Cooling a Proton Exchange Membrane Fuel Cell (PEMFC) using only air flow is gaining popularity as a cooling method due to its low cost and simplicity. Fuel cells that use air cooling are already commercialized up to a power range of a few kW. These fuel cells are limited in current density, and by extension power density, in the amount of heat that can be effectively dissipated by the airflow. By placing a grid in front of the cathode flow channel of the fuel cell stack, experiments have shown the power density could be increased by over 30% as a direct consequence of increased convective cooling. This study uses Computational Fluid Dynamics (CFD) to verify and quantify the effect of a turbulence inducing grid placed at various distances from the cathode channel, as well as under transient operating conditions. At an electrode heat flux of  $2587 \text{ W/m}^2$  the study showed that the average temperature of the Gas Diffusion Layer (GDL) and bipolar plates could be reduced by  $2.5^\circ\text{C}$  with a turbulence inducing grid. A further temperature reduction of the GDL between  $0.3\text{--}2^\circ\text{C}$  was seen by continuously varying the speed of the cooling fan.

*The content of this report is freely available, but publication (with reference) may only be pursued due to agreement with the author.*





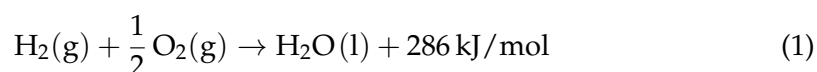
# Contents

<b>Summary</b>	<b>vii</b>
<b>Nomenclature</b>	<b>ix</b>
<b>Preface</b>	<b>xi</b>
<b>1 Introduction</b>	<b>1</b>
1.1 Fuel Cells . . . . .	1
1.1.1 What Is A Fuel Cell? . . . . .	1
1.1.2 Fuel Cell Operation . . . . .	2
1.1.3 Fuel Cell Thermodynamics and Electrochemistry . . . . .	3
1.1.4 Fuel Cell Components . . . . .	8
1.2 Turbulence Inducing Grid . . . . .	10
1.3 Problem Statement . . . . .	11
1.3.1 Methodology . . . . .	11
1.3.2 Previous Work . . . . .	12
<b>2 Computational Fluid Dynamics</b>	<b>15</b>
2.1 Case Presentation . . . . .	15
2.1.1 Computational Domain . . . . .	15
2.1.2 Boundary Conditions . . . . .	19
2.1.3 Mesh . . . . .	21
2.2 Governing Equations and Models . . . . .	25
2.2.1 Governing Equations . . . . .	26
2.2.2 General Transport Equations . . . . .	28
2.2.3 Turbulence Modelling . . . . .	29
2.3 Numerical Method . . . . .	34
2.3.1 Spatial Discretization . . . . .	34
2.3.2 Temporal Discretization . . . . .	34
2.3.3 Solution Algorithm . . . . .	36

<b>3</b>	<b>Results and Discussion</b>	<b>39</b>
3.1	Steady-state . . . . .	40
3.1.1	Effect of Turbulence Inducing Grid and Its Location . . . . .	40
3.1.2	Results Summary . . . . .	46
3.2	Transient . . . . .	47
3.2.1	Effect of Time Dependent Velocity Inlet Under Transient Operating Conditions . . . . .	49
3.2.2	Results summary . . . . .	51
<b>4</b>	<b>Conclusion and Future Work</b>	<b>53</b>
4.1	Conclusion . . . . .	53
4.2	Future Work . . . . .	54
	<b>Bibliography</b>	<b>55</b>

# Summary

Proton exchange membrane fuel cells (PEMFC) are electrochemical devices that convert the molecular energy from its fuel source ( $\text{H}_2$ ) into usable direct current electricity. The overall chemical reaction that takes place within a fuel cell, while accounting for enthalpy changes, is seen below:



Since the reaction is exothermic, energy is released. However, due to irreversible processes only 237.34 kJ/mol of this amount can be converted into electricity. This amount is called the Gibbs free energy of reaction, and sets a limit on the theoretical cell potential that can be achieved for each fuel cell. Theoretically, a fuel cell potential of 1.23 V can be achieved. However, due to activation, ohmic and concentration potential losses the measured voltage will be lower, usually  $< 1 \text{ V}$  depending on the operating current density of the fuel cell. From the 286 kJ/mol, the amount not being used to power an electrical load is converted into heat which heats up the materials of the PEMFC which further decreases efficiency, limiting the current density and deteriorates the fuel cell materials. To overcome this problem of overheating the fuel cell, an effective cooling solution must be used.

One cooling solution that is gaining popularity due to its low cost and simplicity is air-cooling of the fuel cell stack using a conventional fan. These fuel cell systems are already commercialized in the range up to a few kW, in systems where power density (W/kg) is of importance. A major drawback of air-cooled fuel cells is the low maximum current density of around 0.3 - 0.4 A/cm<sup>2</sup> that can be reached due to the inherent limitation of air cooling.

A research group at Aalborg University has shown that placing a grid in front of the cathode channel that induces turbulence, thereby increasing heat transfer within the cathode flow channel, will increase the maximum power density that can be achieved by over 30% [2].

In this thesis, a numerical model using Computational Fluid Dynamics (CFD) is used to investigate this effect at a much higher resolution than what can be achieved under laboratory conditions. For simplicity, only a single fuel cell channel is modelled and symmetry conditions applied to model the stacking of several

fuel cell channels in rows and layers. A mesh of 390.000 cells is used for the steady state analysis, and 60.000 for the transient analysis due to limitations in the computational time available. The  $k-\omega$  SST turbulence model is used for the steady state analysis, while Large Eddy Simulation is used for the transient.

Our results shows that a significant increase in turbulence intensity is seen when a turbulence inducing grid was placed in front of the cathode channel. The smaller the distance between the grid and cathode channel, the more turbulence is produced in the cathode channel. In the best case, the average temperature of the solid materials of the fuel cell could be reduced by  $2.5^{\circ}\text{C}$  at the cost of an additional pressure loss of 4 Pa. From the transient analysis, it is shown that a further reduction in temperature between  $0.3\text{-}2^{\circ}\text{C}$  can be achieved by using a time varying sinusoidal velocity profile as the inlet velocity boundary conditions.

# Nomenclature

## Latin letters

Symbol	Unit	Description
A	m <sup>2</sup>	Area
D	m <sup>2</sup> /s	Diffusivity
E	V	Cell potential
F	C/mol	Faraday constant (96485 C/mol)
G	J	Gibbs free energy
G	m <sup>2</sup> /s <sup>3</sup>	Generation of k/ω
H	J	Enthalpy
i	A/m <sup>2</sup>	Current density
I	A	Current
k	W/m K	Thermal conductivity
k	m <sup>2</sup> /s <sup>2</sup>	Turbulent kinetic energy
n	-	Number of electrons transferred
p	Pa	Pressure
q	C/mol	Charge
Q	W/m <sup>2</sup>	Heat flux
R	J/mol K	Universal gas constant (8.314 J/mol K)
S	J/K	Entropy
S	-	Source term
T	K or °C	Temperature
t	s	Time
u	m/s	Velocity
<b>u</b>	m/s	Velocity vector (u,v,w)
U	m/s	Mean velocity
V	m <sup>3</sup>	Volume
W	J	Work
x	-	Mole fraction
x,y,z	m	Coordinate directions
Y	m <sup>2</sup> /s <sup>3</sup>	Dissipation of k/ω

### Greek letters

Symbol	Unit	Description
$\beta$	-	Bounding factor
$\Gamma$	$\text{m}^2/\text{s}$	Diffusion coefficient
$\delta$	-	Kronecker delta ( $\delta_{ij} = 1$ if $i = j$ and $\delta_{ij} = 0$ if $i \neq j$ )
$\Delta$	-	Change in variable
$\zeta$	-	Stoichiometric coefficient
$\theta$	$^\circ$	Angle
$\mu$	$\text{kg}/\text{m s}$	Dynamic viscosity
$\rho$	$\text{kg}/\text{m}^3$	Density
$\tau$	Pa	Shear stress
$\phi$	-	Transported variable
$\omega$	1/s	Specific rate of turbulent kinetic energy dissipation

### Indices, mathematical symbols and abbreviations

Symbol	Description
f	Face
i	Index
j	Dummy index
el	Electrical
$\nabla \phi$	Gradient of $\phi$
$\nabla \cdot \phi$	Divergence of $\phi$
$\nabla^2$	Laplace operator
CFD	Computational Fluid Dynamics
PEMFC	Proton Exchange Membrane Fuel Cell
MEA	Membrane Electrode Assembly
GDL	Gas Diffusion Layer
NS	Navier-Stokes (equations)
PDE	Partial Differential Equation
FVM	Finite Volume Method
LES	Large Eddy Simulation
RANS	Reynolds Averaged Navier-Stokes (Equations)
CV	Control Volume

# Preface

This is a master's thesis written at the 4th semester of the graduate program Thermal Energy and Process Engineering at Aalborg University, Denmark. The thesis is titled "A computational fluid dynamics study to evaluate the effect of an air-cooled fuel cell stack using a turbulence inducing grid under transient operating conditions" and is supposed to help further advancing the current research carried out at Aalborg University on this topic.

The reader should have a certain level of knowledge regarding computational fluid dynamics, heat transfer and fuel cell systems.

The author would like to thank his counselors: Associate Professor Torsten Berning and Associate Professor Chungen Yin from Aalborg University for their help and collaboration in writing this thesis, as well as the department of energy technology at Aalborg University for facilitating a good study and work environment.

Aalborg University, May 30, 2019

A handwritten signature in black ink, appearing to read 'Alex', with a long horizontal stroke extending to the right.

---

Alexander Strømfeldt Lind  
<alind14@student.aau.dk>





# Chapter 1

## Introduction

### 1.1 Fuel Cells

In this section, fuel cell fundamentals will be presented. First a brief overview of a fuel cell its function and history in Sec. 1.1.1. Then a description of fuel cell operating principles in Sec. 1.1.2 which will lead to a thermodynamic analysis in Sec. 1.1.3. At the end of the section a more detailed description of the various components within a fuel cell will be presented in Sec. 1.1.4. The components described in Sec. 1.1.4 will have to be modelled in the Computational Fluid Dynamics (CFD) model described in Ch. 2.

#### 1.1.1 What Is A Fuel Cell?

Fuel cells are an electrochemical energy converter which converts electrochemical energy from its fuel into usable Direct Current (DC) electricity. It accomplishes this energy conversion in only one stage, which compared to conventional fuel to energy converting processes, e.g. Rankine cycles, makes it very efficient. In simple terms, a fuel cell can be viewed as a black box model where hydrogen and oxygen enters and reacts, and the products are waste heat, water and DC electricity (See Fig. 1.1). The first fuel cell was invented in 1839, attributed to Sir William Grove. However, it was merely seen as a scientific curiosity until Francis T. Bacon started work on developing a practical fuel cell in 1937, and by 1950 a 6kW fuel cell was developed. Fuel cells were then used during the 1950's and 60's in the Gemini and Apollo space programs to generate electricity aboard spacecrafts to power the life support systems, guidance and communication hardware. [1]

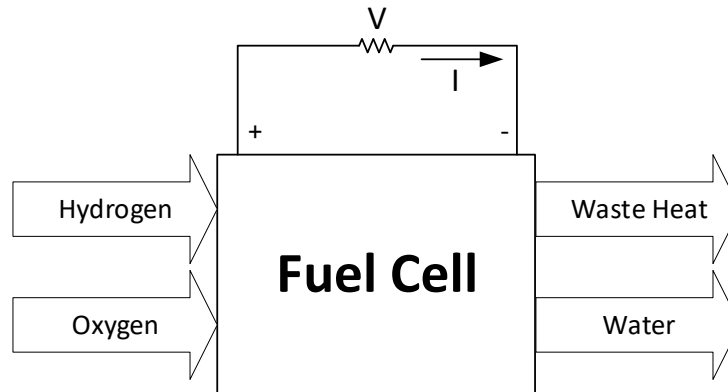


**Figure 1.1:** Working principle of a fuel cell

Since then, fuel cells have found its way into many different industries. The high power to weight ratio makes the technology suitable for the transportation sector as zero emission fuels are becoming more desired. Fuel cells may also play a role in developing high range drone aircrafts, as the energy density of hydrogen fuel is much higher than what can be achieved with the current available electrolytic batteries. A lightweight and cheap cooling solution would be required for such applications, since cooling systems for fuel cells make up a significant percentage of its total weight. The air-cooled fuel cell using a turbulence inducing grid, which will be presented in Sec. 1.2 may be a solution to this problem.

### 1.1.2 Fuel Cell Operation

The core component of a fuel cell is the Membrane Electrode Assembly (MEA) which produces the electrochemical reaction needed to separate electrons for use in an electric circuit. In the typical 5-layer MEA (MEA5) seen in Fig. 1.2, hydrogen gas ( $H_2$ ) is split into protons and electrons in the anode catalyst layer. The protons can then travel through the proton exchange membrane (PEM) which is impermeable to gasses, while the electrons travel through a external circuit to reach the cathode catalyst layer. Oxygen, electrons and protons combine in the cathode catalyst layer to form liquid water or steam depending on the operation temperature.

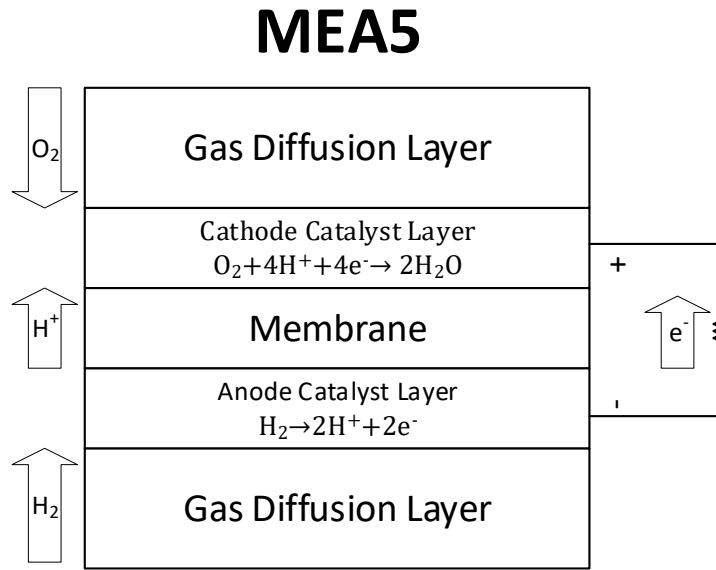
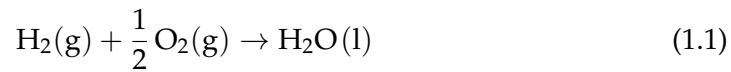


Figure 1.2: Operation of a fuel cell

Combining the two half reactions seen in Fig. 1.2 the overall fuel cell reaction is seen in Eq. 1.1.



### 1.1.3 Fuel Cell Thermodynamics and Electrochemistry

As mentioned earlier, fuel cells are electrochemical energy converters and must obey the laws of thermodynamics. This section will present a thermodynamic analysis of fuel cell operations in order to determine the amount of heat that is generated under operation. The heat generation will need to be modelled in the computational fluid dynamics analysis presented in Ch. 2.

#### Heat of Reaction

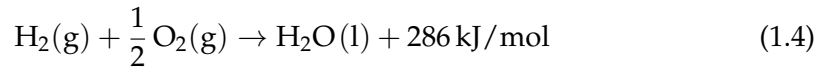
The overall reaction seen in Eq. 1.1 is identical to the combustion of hydrogen. Therefore, heat must be produced from this reaction since it is exothermic. The heat generated is the difference between the enthalpy of formation between the products and reactants:

$$\Delta H = \Delta H_{f,\text{H}_2\text{O}} - \left( \Delta H_{f,\text{H}_2} + \frac{1}{2} \Delta H_{f,\text{O}_2} \right) \quad (1.2)$$

The enthalpy of formation of liquid water is  $-286 \text{ kJ/mol}$  (At  $25^\circ\text{C}$ ) while for elements in their standard state it is per definition equal to zero. The calculation then becomes:

$$\Delta H = -286 \text{ kJ/mol} - (0 + 0) = -286 \text{ kJ/mol} \quad (1.3)$$

The negative sign in Eq. 1.3 means that energy is being released and is therefore exothermic. The overall reaction in Eq. 1.1 can then be rewritten with heat generation accounted for:



In a fuel cell, the waste heat generated must be carried out by the reactant air. At least for an air-cooled system.

### Gibbs Free Energy

Based on the enthalpy of formation,  $286 \text{ kJ/mol}$  could be released in the form of heat for Eq. 1.4. However, the function of a fuel cell is to produce electricity, not heat. Obviously, not all this energy can be converted into electricity. To calculate the amount of electricity that can be generated, a Gibbs free energy calculation can be performed:

$$\Delta G = \Delta H - T\Delta S \quad (1.5)$$

From Eq. 1.5 it can be seen that there are some irreversible losses due to the creation of entropy. The entropy of formation can be calculated similarly to the enthalpy of formation:

$$\Delta S = \Delta S_{f,\text{H}_2\text{O}} - \left( \Delta S_{f,\text{H}_2} + \frac{1}{2} \Delta S_{f,\text{O}_2} \right) \quad (1.6)$$

Using tabulated values for  $\Delta S_f$  at  $25^\circ\text{C}$   $\Delta S$  can be calculated:

$$\Delta S = 0.069 \frac{\text{kJ}}{\text{mol} \cdot \text{K}} - \left( 0.131 \frac{\text{kJ}}{\text{mol} \cdot \text{K}} + \frac{1}{2} 0.205 \frac{\text{kJ}}{\text{mol} \cdot \text{K}} \right) = -0.165 \frac{\text{kJ}}{\text{mol} \cdot \text{K}} \quad (1.7)$$

At  $25^\circ\text{C}$ , Gibbs free energy then becomes:

$$\Delta G = -286 \text{ kJ/mol} - 298.15 \text{ K} \cdot -0.165 \frac{\text{kJ}}{\text{mol} \cdot \text{K}} = 237.34 \text{ kJ/mol} \quad (1.8)$$

From Eq. 1.8 it can be seen that out of an available  $286 \text{ kJ/mol}$  of energy, only  $237.34 \text{ kJ/mol}$  can be converted into electricity and the remaining energy will be converted to heat. These values will depend on the temperature of the reaction.

### Theoretical Fuel Cell Potential

Generally, electrical work is the product of charge and potential:

$$W_{el} = qE \quad (1.9)$$

The charge transferred per mole of  $H_2$  in a fuel cell reaction is given by Eq. 1.10.

$$q = nF \quad (1.10)$$

Where,

$n$  is the number of electrons per molecule of  $H_2$  which is 2.

$F$  is the Faraday constant  $\left(96\,485\text{ C mol}^{-1}\right)$

Electrical work for a fuel cell is then given by combining Eq. 1.9 & 1.10:

$$W_{el} = nFE \quad (1.11)$$

As explained in Sec. 1.1.3, the maximum electrical work in a fuel cell reaction is the Gibbs free energy, therefore:

$$-\Delta G = nFe \rightarrow E = \frac{-\Delta G}{nF} = \frac{237\,340\text{ J mol}^{-1}}{2 \cdot 96\,485\text{ C mol}^{-1}} = 1.23\text{ V} \quad (1.12)$$

As shown, the theoretical fuel cell potential is 1.23 V, however the actual voltage during operation will be lower due to unavoidable losses as will be explained in the next section.

### Voltage Losses and Polarization Curve

The maximum theoretical fuel cell potential based on the laws of thermodynamics was calculated to be 1.23 V. If a fuel cell has available reactants, but the external electrical circuit is not closed (Fig. 1.3-a) then no current will be generated and you would expect to measure 1.23 V on a voltmeter. However, in practice the measured open circuit voltage for a fuel cell will typically be around 1 V, meaning that there are voltage losses even when no current is generated. When current is generated after closing the electrical circuit and connecting an electrical load (Fig. 1.3-b), the voltage is expected to be even lower due to additional current dependent voltage losses.

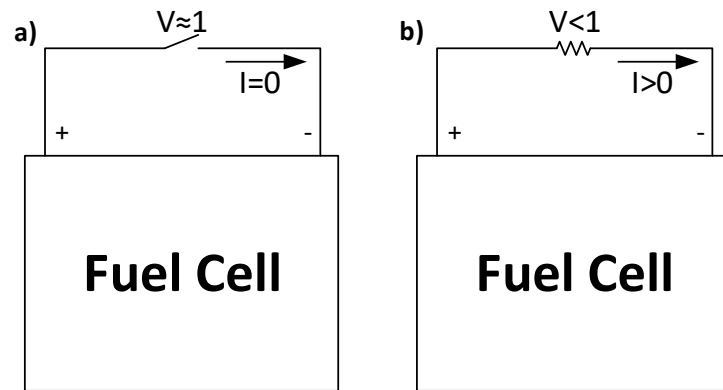


Figure 1.3: Fuel cell potential for a) open circuit b) under resistive load

The three main factors that cause voltage losses in fuel cells are:

**Activation losses:** Due to the 'slowness' of reactions taking place at both electrode surfaces. This loss factor is dominant in the low current density region, and becomes less dominant at higher current densities.

**Ohmic losses:** Due to the resistance to ion flow in the electrolyte as well as electron resistance within the electrically conductive fuel cell components. The resistive losses can be modelled using Ohm's law  $\Delta V = iR$  and is therefore linear proportional to the current density  $i$ .

**Concentration losses:** Due to the rapid consumption of reactants at the electrode surfaces. At maximum current densities, the reactant concentration near the electrode is practically zero so they are consumed as soon as they reach the electrode. This 'starvation' of reactants leads to a voltage loss that dominates at high current densities.

When designing a fuel cell, one must consider all these voltage losses and try to minimize them as much as possible. To visualize the fuel cell performance while accounting for voltage losses, a polarization curve is used. A polarization curve shows the cell potential (or voltage) as a function of current density. An example of a polarization curve is given in Fig. 1.4.

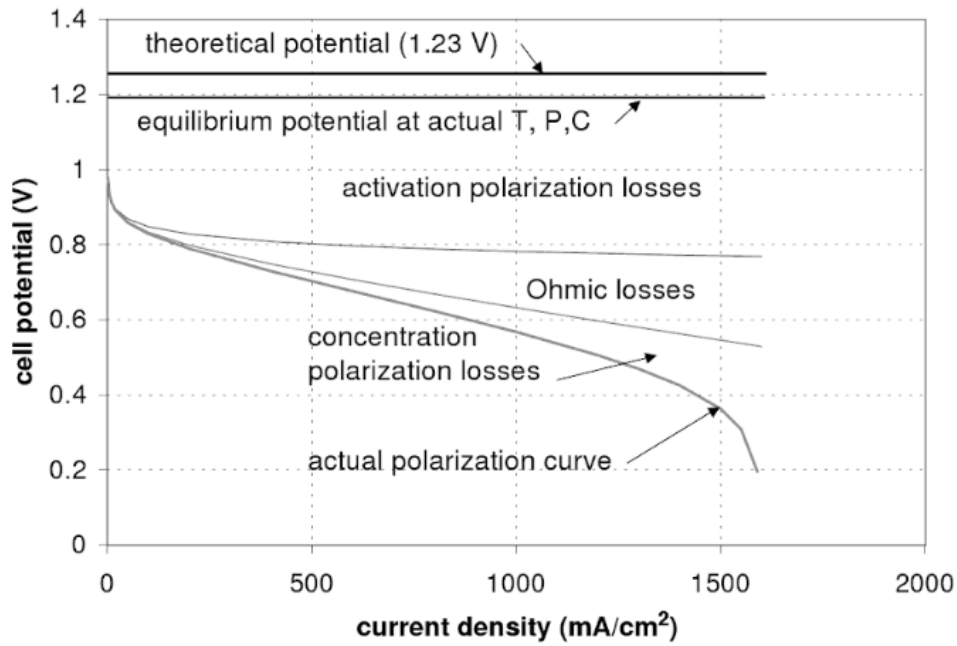


Figure 1.4: Fuel cell polarization curve with voltage losses. Source: [1]

The fuel cell that will be used to calculate heat generation for the CFD study in Ch. 2 is the Mark1020 ACS™ fuel cell stack by Ballard Power Systems Inc. The polarization curve for this fuel cell stack is given in Fig. 1.5.

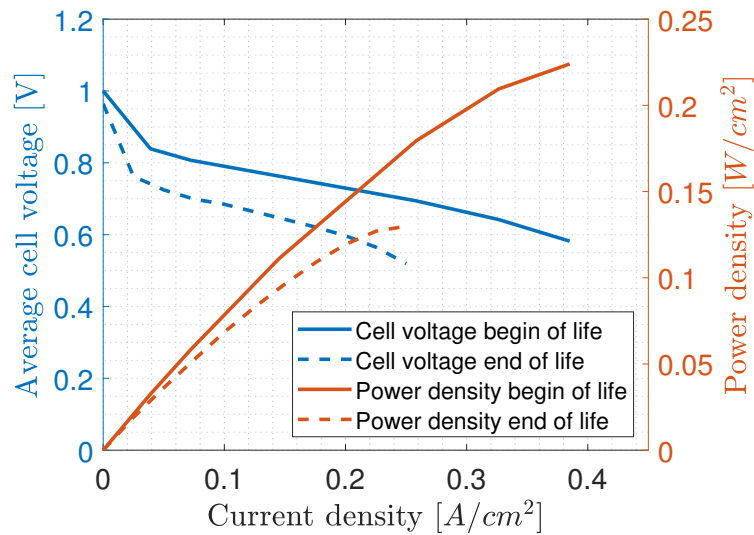
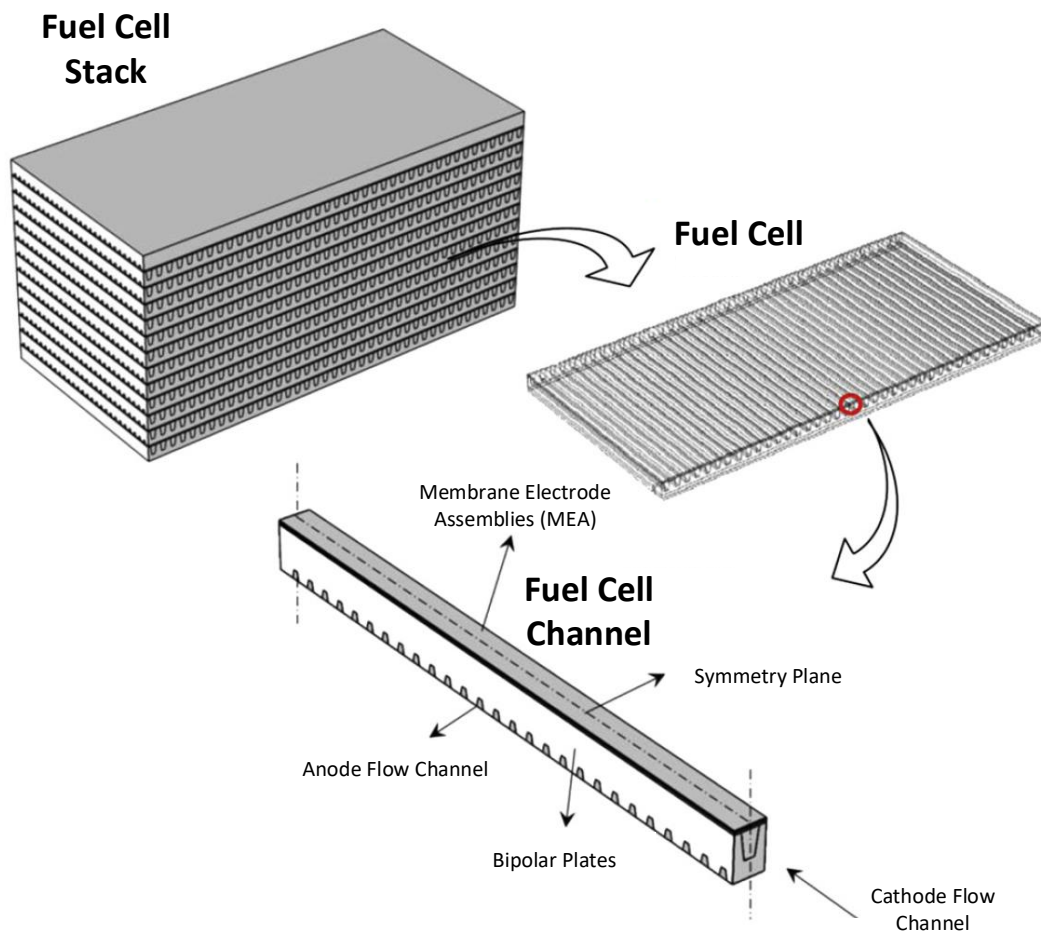


Figure 1.5: Mark1020 ACS™ fuel cell stack polarization curve at beginning and end of service life.

### 1.1.4 Fuel Cell Components

Commercially, fuel cells are typically arranged in a fuel cell stack in order to provide the electrical potential and power output required for applications in the transportation, aviation and aerospace sectors. A fuel cell stack can be decomposed into fuel cell layers, and each layer contains several fuel cell channels (See Fig. 1.6). For the CFD study in Ch. 2, only a single fuel cell channel will be simulated in order to keep computational time down. The fuel cell channels are in a stacked symmetric arrangement within the fuel cell stack.



**Figure 1.6:** Structure of a fuel cell stack. [10]

Looking at Fig. 1.6, the fuel cell channel is made up of two primary components, the MEA and bipolar plates. In Fig. 1.2 the structure of the MEA is seen to consist of a cathode and anode electrode surface, a proton exchange membrane as well as two gas diffusion layers. For simplicity only the cathode side gas diffusion



layer will be modelled in the CFD analysis, since chemical reactions are not implemented in the model only the resultant heat flux. The function and properties of the two important fuel cell components will now be presented:

### Gas Diffusion Layer

The GDL is the layer between the catalyst layer and the bipolar plates in the MEA, and has the following functions:

- Pathway for reactant gases between the flow field channels and the catalyst layer. Therefore, must be porous.
- Electrically connects the catalyst later and the bipolar plate.
- Conducts heat from the catalyst layer to the bipolar plate.

The GDL is made of Carbon-Carbon composite paper, which has the mechanical strength, conductivity and porosity required to function as a GDL. The material properties used for the GDL in the CFD case can be seen in Tab. 1.1 below.

Gas Diffusion Layer		
Property	Value	Unit
Density	450	kg / m <sup>3</sup>
Specific heat	900	J kg <sup>-1</sup> K <sup>-1</sup>
Thermal Conductivity	1.7	W m <sup>-1</sup> K <sup>-1</sup>
Surface Roughness	8	μm

**Table 1.1:** Gas Diffusion Layer Properties [11]

### Bipolar Plates

The bipolar plates have several functions in an operating PEMFC [1]:

- Connects adjacent cells in a series electrical connection, therefore must be electrically conductive.
- Separation of gases. Therefore, must be impermeable to gases.
- Structural support.
- Conduction of heat away from active cells. Therefore must be thermally conductive.
- Houses the flow field channel.

The first material used for bipolar plates, which is still commonly used in laboratory fuel cells is graphite. The material properties used for the bipolar plate in the CFD case can be seen in Tab. 1.2 below.

Bipolar Plates		
Property	Value	Unit
Density	1970	$\text{kg} / \text{m}^3$
Specific heat	720	$\text{J kg}^{-1} \text{K}^{-1}$
Thermal Conductivity	20.5	$\text{W m}^{-1} \text{K}^{-1}$
Surface Roughness	0	$\mu\text{m}$

**Table 1.2:** Bipolar Plate Physical Properties [1]

## 1.2 Turbulence Inducing Grid

Grids have paradoxically been used to both produce and reduce turbulence in fluid flow, by either creating or eliminating velocity or pressure nonuniformities [8]. For this report, it is the turbulence creation aspect of grids that are interesting. The function of a turbulence inducing grid (Fig. 1.7-b) is to turn a uniform upstream velocity profile (Fig. 1.7-a) into a nonuniform velocity profile downstream (Fig. 1.7-c) which will then allow the flow to transition from laminar into turbulent which is dominated by swirling eddies (Fig. 1.7-d). It is well understood that turbulent flow increases heat and mass transport, and therefore could be convenient to create on demand. For certain applications however, the additional pressure loss will reduce the effectiveness of a grid.

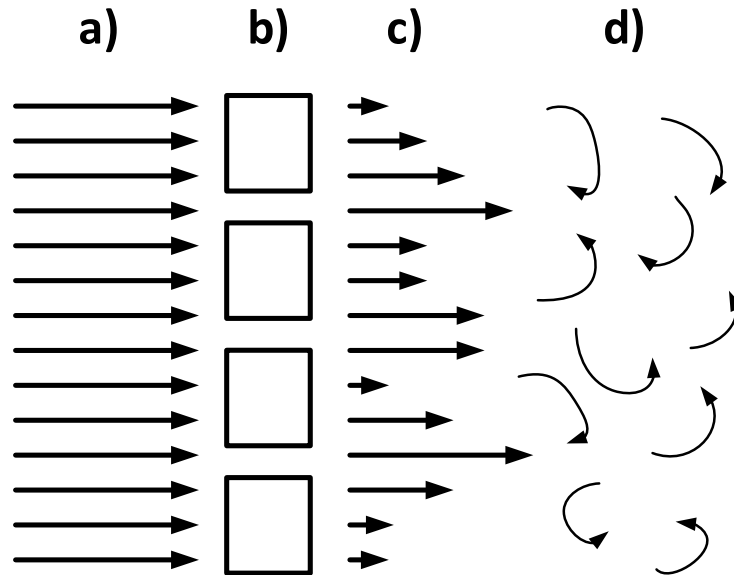


**Figure 1.7:** Illustration of **a)** uniform upstream velocity profile **b)** turbulence inducing grid **c)** nonuniform downstream velocity profile **d)** swirling eddies

Inside the cathode flow channel shown in Fig. 1.6 heat needs to be removed by air when using an air-cooled fuel cell stack, in order to keep the temperature of the MEA and bipolar plates below maximum operating temperatures. Heat is created by the chemical reactions inside the MEA and travels through conduction to the gas diffusion layer and bipolar plates. If a grid could be used to induce turbulence into the air flow downstream of the cathode flow channel, it could be expected that convective heat transfer would increase in some areas of the flow channel. This would reduce the operating temperature of the fuel cell channel, as more heat is transferred to the air from the GDL and bipolar plates, allowing for an increase in current/power density (See Fig. 1.9).

### 1.3 Problem Statement

The objective of this report is to investigate the effect a turbulence inducing grid has on the heat transfer within the cathode flow channel of a fuel cell channel. The distance between the grid and the inlet of the cathode flow channel is a design variable that must be considered. Based on the stated objective, the following problem statement is proposed:

*Will the presence of a turbulence inducing grid increase convective heat transfer in a fuel cell channel resulting in lower operating temperatures, and will a fluctuating velocity profile further improve heat transfer?*

The following research questions will also be addressed in the report:

1. How should the expected turbulence that is induced by the grid be modelled?
2. How much does the distance between the grid and cathode flow channel affect heat transfer in the channel?
3. Could you further improve heat transfer by continuously varying the speed of the fan cooling the fuel cell?

The variables used to answer these questions will be the temperatures at various locations of the domain, as well as the turbulence intensity (See Eq. 3.1)

#### 1.3.1 Methodology

To answer the questions raised in the problem statement, an acceptable methodology must be used. Several different methodologies could be used for this case:

**Experimental:** An experiment could be designed in order to analyze the effect of the turbulence inducing grid on a commercial type fuel cell stack. However,

such experiments have already been conducted previously [3]. The conclusions made from these experiments was that the power density of a fuel cell could be increased by up to 30%, due to the heat transfer increase between the cathode channel layer and the air in the PEMFC. The disadvantage of such an approach, is the limited amount of data points that can be obtained. In order to get a complete understanding of the velocity and temperature field, another method would be preferred.

**Analytical:** The equations that describe the motion of viscous fluids are the Navier-Stokes (NS) equation. The NS equations are partial differential equations (PDE) and consists of three momentum conservation equation and one for continuity along with a energy equation. These equations will be discussed further in Sec. 2.2.1. An exact analytical solution to the NS equations exists only for a few degenerate cases, and often relies on assumptions of non-viscosity, fully laminar flow etc. For this case, an exact solution to the NS equations cannot be found so another method must be used.

**Numerical:** The goal of a numerical study, is to give an approximate yet accurate solution to complex flow problems where no analytical solution can be found. In Computational Fluid Dynamics (CFD) this is usually accomplished using the finite volume method (FVM) for representing and evaluating the governing PDE's in the form of algebraic equations. All relevant equations need to be solved at discrete places in the defined geometry, dependent on the solving scheme used.

In order to apply FVM, the geometry of interest will need to be subdivided into discrete defined volumes. This process is called 'meshing'. The number of volumes used in a CFD analysis, will vary depending on factors such as accuracy requirements, computational hardware availability and geometry complexity.

A numerical methodology, in the form of CFD and FVM is the considered to be the best approach to answer the questions raised in the problem statement, and will be used throughout this report.

### 1.3.2 Previous Work

#### Experimental work

Experimental work was performed by a research group at Aalborg University [3], where a variety of turbulence inducing grids was placed in front of the cathode flow channel of a Ballard Power Systems Mark 1020 ACS<sup>TM</sup> air-cooled proton exchange membrane fuel cell in order to study its effect on the fuel cell operation. A diagram of the test setup used can be seen in Fig. 1.8.

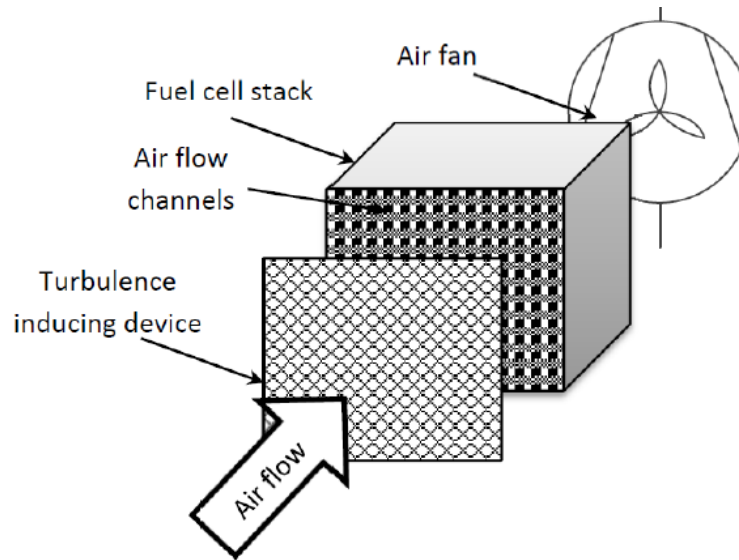


**Figure 1.8:** Experimental setup used to test the effect of a turbulence inducing grid

The experiments showed a drastic improvement in performance, when compared to the performance with no grid. In the best case, an increase in power density of over 30% was seen. Since the limiting performance factor for an air-cooled proton exchange membrane fuel cell is the cooling, it was concluded that this performance increase was solely due to presence of a turbulence inducing grid. The polarization curve of the fuel cell with and without the grid, presented in their paper, is seen in Fig. 1.9.

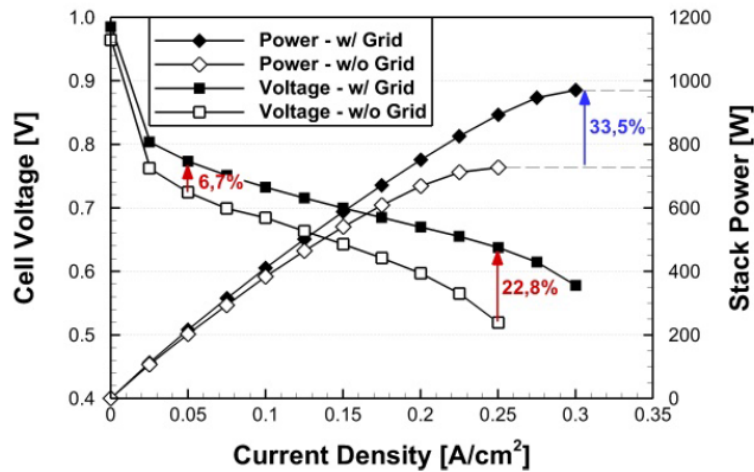


**Figure 1.9:** Polarization curve for the Ballard Power Systems Mark 1020 ACST<sup>TM</sup> air-cooled proton exchange membrane fuel cell with and without a grid [3]

### CFD study

As part of a master's thesis at Aalborg University, two graduates made a CFD study in order to try and replicate the drastic performance increase seen in the experimental work described above [4]. However, the results showed only an negligible impact on the maximum temperature of the PEMFC when using a turbulence inducing grid ( $<1$  K). On further review, it was found that some of assumptions used for the study was unjustified, such as the assumption of constant density and heat capacity of air.

Also, the mesh quality and fineness may not have been adequate to accurately capture the flow structures within the cathode flow channel as well as properly modelling the heat conduction in the solid region of the bipolar plates. A comparison between the mesh used for the previous CFD study and the one that will be presented in this report is given in Fig. 1.10.

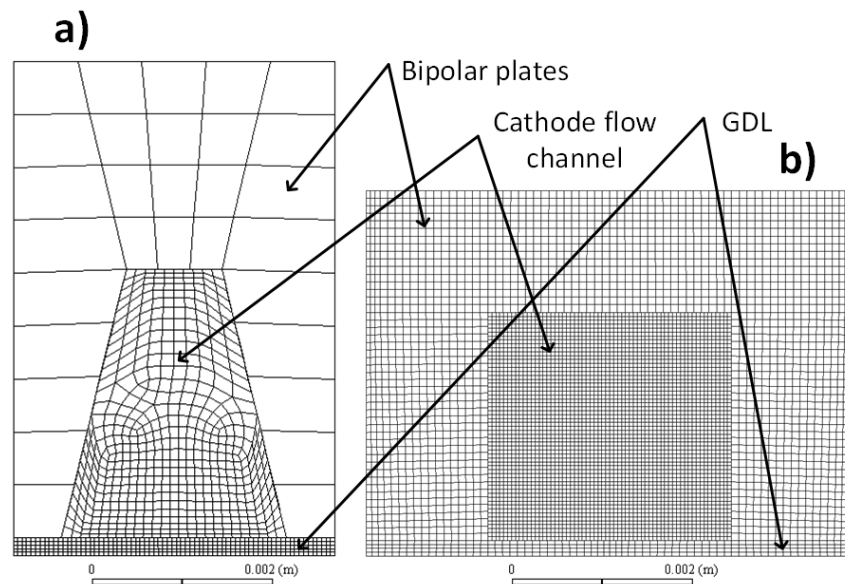


**Figure 1.10:** Comparison of the mesh used for a) Previous CFD study [4] b) This report

The geometry of the fuel cell has been changed slightly for this report. This was done in order to create a structured mesh of a higher cell quality. However, steps were made to ensure that the hydraulic diameter of the new geometry is like that of the old ( $\approx 1$ mm). It was decided that it was worth redoing the CFD study using an improved mesh and modelling technique. This thesis is that attempt.

## Chapter 2

# Computational Fluid Dynamics

### 2.1 Case Presentation

In Ch. 1 the function and structure of a PEMFC were introduced. In summary, a PEMFC converts the chemical energy stored in hydrogen bonds into electrical energy that could be used to power a circuit, charge a battery etc. This process is exothermic, so heat is released which increases the temperature of the PEMFC, leading to a performance drop and increased deterioration of the PEMFC.

The implementation of a turbulence inducing grid, should increase the convective heat transfer inside the cathode channel and allow more heat to be transported away from the PEMFC. The geometry used for the analysis, must be able to capture both the downstream effect of the turbulence inducing grid as well as the entire cathode channel domain, both solid and fluid.

#### 2.1.1 Computational Domain

The full geometry that will be used in the CFD case, contains the bipolar plates, gas diffusion layer, turbulence inducing grid as and the fluid domain. The full geometry is seen in Fig. 2.1.

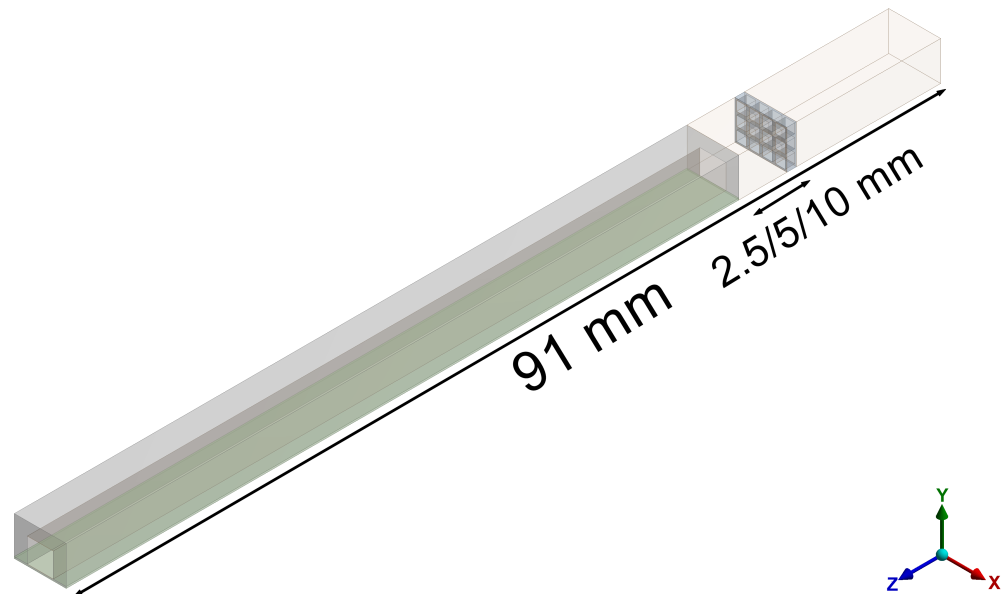


Figure 2.1: Full geometry

### Bipolar Plates

The geometry of the bipolar plates is seen in Fig. 2.2 below.

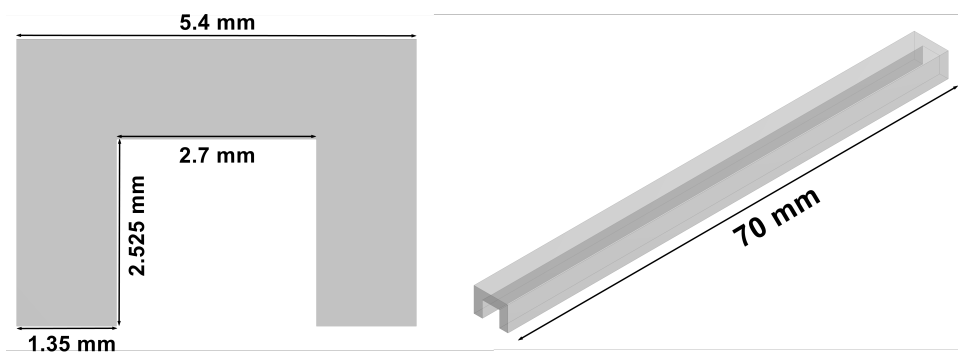


Figure 2.2: Bipolar Plate Geometry

### Gas Diffusion Layer (GDL)

The geometry of the GDL is seen in Fig. 2.3 below.



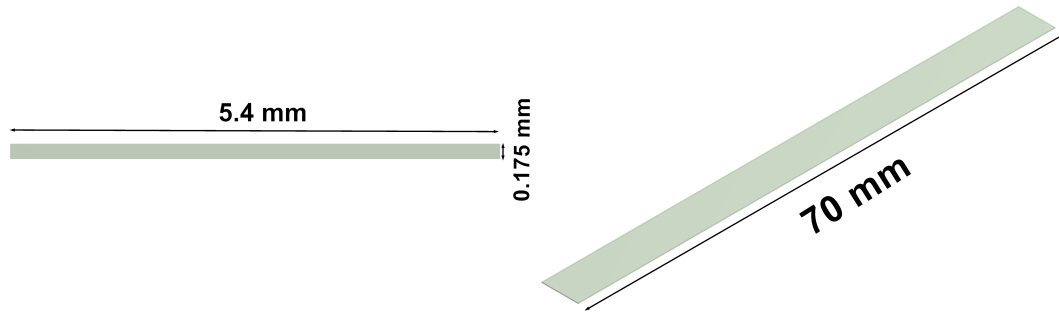


Figure 2.3: Gas Diffusion Layer Geometry

### Turbulence Inducing Grid

The geometry of the turbulence inducing grid is seen in Fig. 2.4 below.

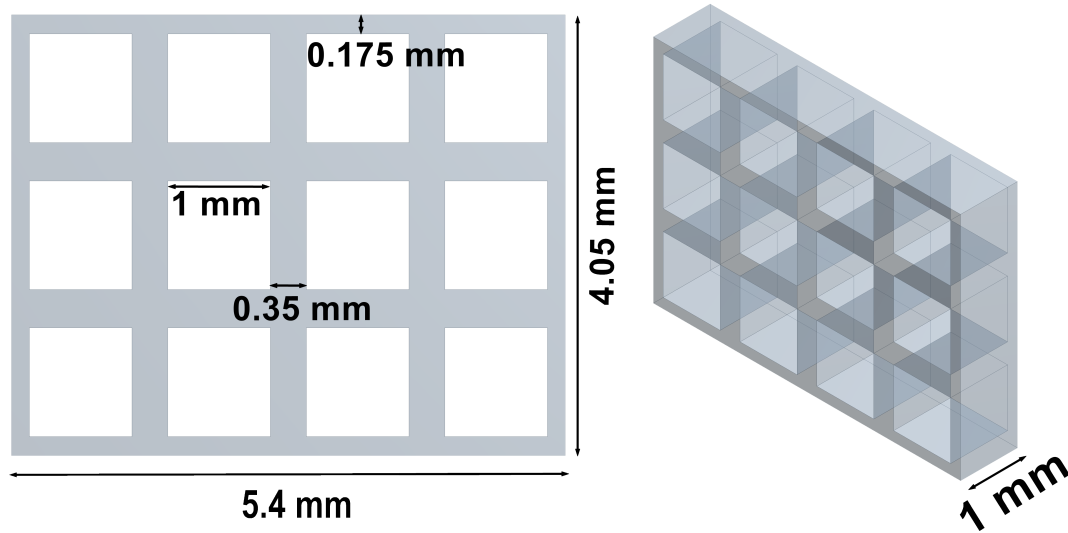


Figure 2.4: Turbulence Inducing Grid Geometry

The turbulence inducing grid will be introduced to the flow field at varying distances from the flow channel and compared to the base case without any grid. Previous studies have found that the critical Reynolds Number for a turbulence grid to introduce downstream turbulence is  $Re_{cr} \approx 175$  [6]. According to the authors, at  $Re < Re_{cr}$  the effect of the grid are indeterminate.

The physical properties of the grid is seen below in Tab. 2.1.

Turbulence Inducing Grid		
Property	Value	Unit
Density	2719	$\text{kg} / \text{m}^3$
Specific heat	871	$\text{J kg}^{-1} \text{K}^{-1}$
Thermal Conductivity	202.4	$\text{W m}^{-1} \text{K}^{-1}$
Surface Roughness	0	$\mu\text{m}$
Grid Fill Factor	54.8	%

**Table 2.1:** Turbulence Inducing Grid Properties

### Symmetry

In order to minimize the number of cells in the computational domain, a symmetry plane can be used on the geometry seen in Fig. 2.1 in the Y-Z plane. In order to use a symmetry plane, a RANS based isotropic turbulence models must be used, such as the  $k-\epsilon$  and  $k-\omega$  since resolved eddies are an-isotropic in nature. For unsteady turbulent flow calculations, such as DNS and Large Eddy Simulation (LES) a symmetry plane cannot be used without introducing an error. The geometry that will be used when symmetry can be applied is seen in Fig. 2.5.

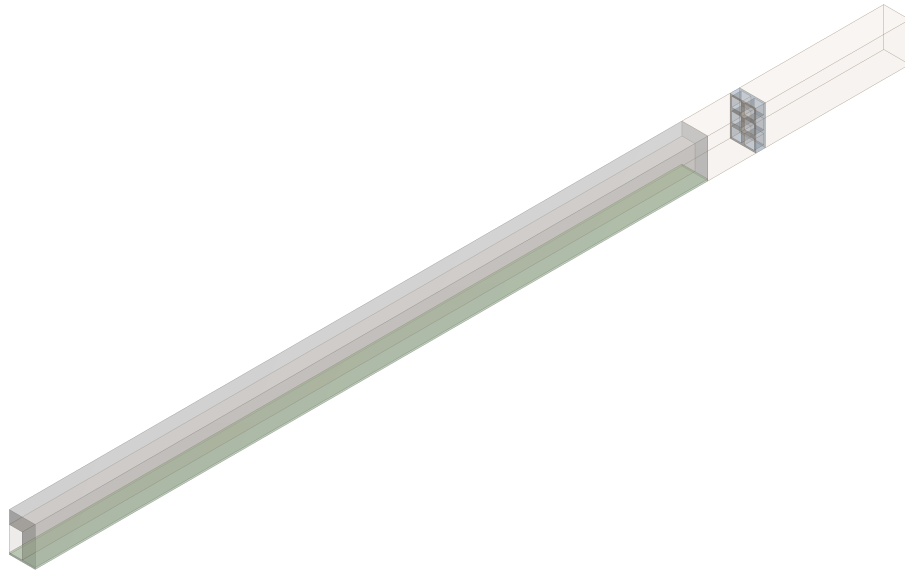


**Figure 2.5:** Full geometry with a symmetry plane

### 2.1.2 Boundary Conditions

The location of the boundary conditions for the geometry is seen in Fig. 2.6. The type of boundary condition used, and its value is listed in Tab. 2.2.

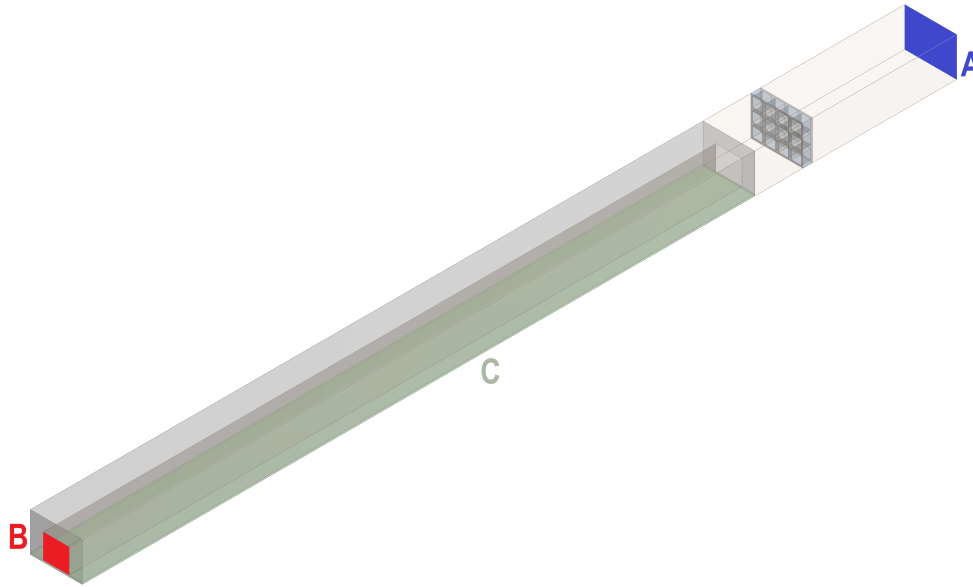


Figure 2.6: Placement of boundary conditions

Boundary Conditions			
Name	BC	Type	Value
A. Inlet	Velocity	Dirichlet	1.05 m/s
	Temperature	Dirichlet	20 °C
	k and $\omega$	Dirichlet	0.0001
B. Outlet	Pressure	Dirichlet	0 Pa
C. GDL	Heat Flux	Neumann	2587 W/m <sup>2</sup>
Remaining	Symmetry	Neumann	All fluxes = 0

Table 2.2: Boundary conditions

How the values for the velocity inlet and heat flux was found, will be explained in the following sections.

### Calculation of GDL heat flux

For a fuel cell stack that combines hydrogen and oxygen with a by-product of water in a gaseous state, the heat generated can be modelled as [1]:

$$\dot{Q} = (1.254 \text{ V} - E_{\text{Cell}}) I \cdot N_{\text{Cells}} \quad (2.1)$$

Where, 1.254 V is the electrolyzer voltage.  $E_{\text{Cell}}$  is the cell voltage,  $N_{\text{Cells}}$  is the number of cells in the fuel cell stack and  $I$  is the stack current. Since the CFD case will only contain a single cell  $I \cdot N_{\text{Cells}}$  will be substituted with the current density  $i$  ( $\text{A}/\text{m}^2$ ). Eq. 2.1 then becomes:

$$\dot{Q} = (1.254 \text{ V} - E_{\text{Cell}}) i \quad (2.2)$$

For a fuel cell, there is a dependency between cell voltage and current density. This dependency is related to the voltage losses in the fuel cell stack. A polarization curve is used to show this dependency for a given fuel cell stack. This was further explained in Sec. 1.1.2.

For the CFD case, a high current density of  $0.385 \text{ A}/\text{cm}^2$  will be used. This value is assumed to give a cell voltage of  $0.582 \text{ V}$ , according to Fig. 1.5 in Sec. 1.1.2. Using Eq. 2.2 and the values mentioned, the heat flux into the GDL is calculated:

$$\dot{Q} = (1.254 \text{ V} - 0.582 \text{ V}) 0.385 \text{ A}/\text{cm}^2 = 0.2587 \text{ W}/\text{cm}^2 = 2587 \text{ W}/\text{m}^2 \quad (2.3)$$

### Calculation of velocity inlet value

The required inlet flow velocity for a fuel cell channel, in order to achieve a desired stoichiometric flow ratio, can be calculated using Eq. 2.4[4][2].

$$u_{\text{in}} = \zeta \frac{i}{4F} A_{\text{GDL}} \frac{R \cdot T_{\text{in}}}{x_{\text{O}_2, \text{in}} p_{\text{in}} A_{\text{ch}}} = 3.36 \text{ m/s} \quad (2.4)$$

This value is found using the parameters listed in Tab. 2.4.

Name	Symbol	Value	Unit
Stoichiometry	$\zeta$	50	-
Current density	$i$	3850	A/m <sup>2</sup>
Faraday Constant	$F$	96485.33	C/mol
GDL surface area	$A_{GDL}$	$3.78 \times 10^{-4}$	m <sup>2</sup>
Gas constant	$R$	8.314472	J/K · mol
Inlet temperature	$T_{in}$	293.15	K
Oxygen Mole Fraction	$x_{O_2,in}$	0.21	-
Pressure at inlet	$p_{in}$	101325	Pa
Cross sectional area of cathode channel	$A_{ch}$	$6.82 \times 10^{-6}$	m <sup>2</sup>

**Table 2.3:** Parameters used for inlet velocity calculation

Since the inlet velocity value is specified on surface A in Fig. 2.6, a corrected velocity must be calculated since the cross-sectional area of the channel is not equal to the area of surface A. This can easily be done using the following relation:

$$\frac{u_1}{u_2} = \frac{A_1}{A_2} \quad (2.5)$$

This relation is valid because with symmetry boundary conditions no air will escape the volume seen in Fig. 2.1, due to the zero flux condition. Therefore, all air entering from surface A must enter the cathode channel. The corrected velocity will then be:

$$u_{bc} = u_{ch} \frac{A_{ch}}{A_{bc}} = 3.36 \text{ m/s} \frac{6.82 \times 10^{-6} \text{ m}^2}{21.87 \times 10^{-6} \text{ m}^2} = 1.05 \text{ m/s} \quad (2.6)$$

### 2.1.3 Mesh

Spatial discretization of the computational domain, is an important part of the pre-processing of any computational fluid dynamics study. The equations that are used to spatially discretize the domain was presented in Sec. 2.3.1. In this section the meshes used to generate the results presented in Ch. 3, will be presented. The general mesh generation procedure can be summed up by the flow chart seen in Fig. 2.7 [9].



**Figure 2.7:** General mesh generation methodology

The CFD software used in this report is the student version of Ansys Fluent 19.2. There is a cell limitation in this version, since it is freely available to engineering students worldwide. The limitation of 512,000 cells requires cell usage efficiency.

The process of generating meshes can broadly be categorized into two categories with their own advantages and disadvantages:

**Structured:** A structured mesh consists of defined sets of hexahedral elements with point-to-point connectivity. This type of mesh has a defined, and therefore predictable, neighborhood arrangement. Structured meshes usually give a better convergence rate and better resolution, but can be difficult to implement on complex geometries.

**Unstructured:** An unstructured mesh has non-repeating irregular connectivity between nodal points. It usually consists of tetrahedral elements. Neighborhood arrangements are unique and must therefore be stored in memory. An unstructured mesh can easily be generated on complex geometries, and is therefore the method of choice for automatic meshing algorithms.

An example on the difference between a structured and an unstructured mesh can be seen below in Fig. 2.8.

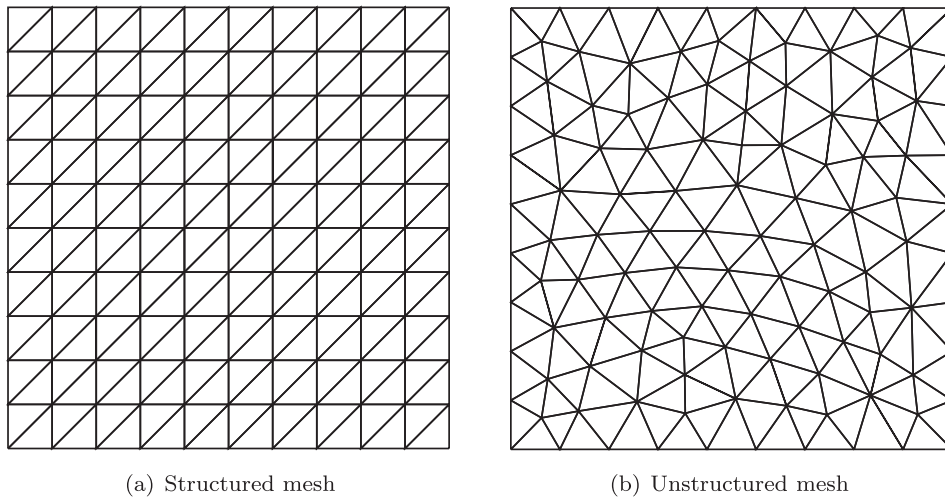


**Figure 2.8:** Example of a structured and unstructured triangular mesh

Steps were taken to ensure a relative simple geometry for this case, therefore a structured mesh is used for all calculations to increase numerical accuracy and convergence rate. A good convergence rate is especially important for the transient analysis that will be conducted in order to reduce the amount of iterations required per time-step.

### Skewness

Cell skewness is an important quality measure for a generated mesh, since highly skewed cells will cause convergence instabilities. The reason for the instability, is that face fluxes are calculated under the assumption that the vector between cell centers are normal to their common face. If a cell is skewed, this criterion is not fulfilled and wrong variable values are calculated, preventing numerical convergence.

The difference between an ideal equiangular cell and a skewed cell is seen in Fig. 2.9.

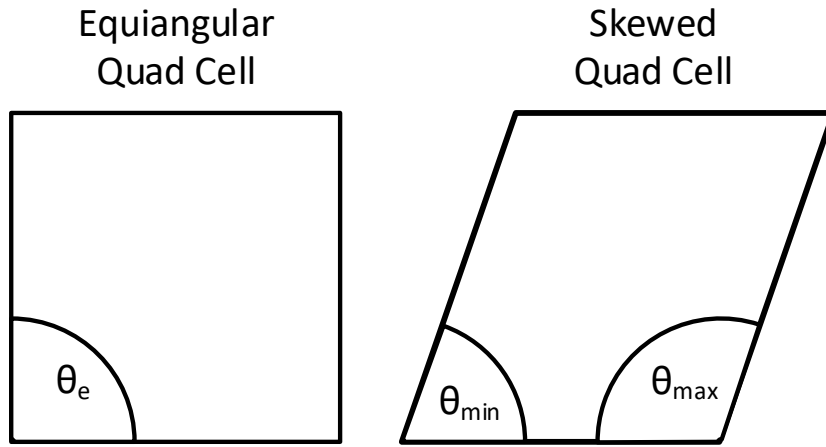


**Figure 2.9:** Ideal and skewed quad cell

The skewness values for the generated meshed presented in the next section is calculated in the following manner:

$$\text{Skewness} = \max \left( \frac{\theta_{max} - \theta_e}{180^\circ - \theta_e}, \frac{\theta_e - \theta_{min}}{\theta_e} \right) \quad (2.7)$$

### Generated meshes

Not all meshes are created equally. Therefore, certain properties related to the mesh quality must be tracked in order to avoid numerical and convergence issues.

This section will contain a brief account of some of these properties for the meshes used for both the steady-state as well as the transient analysis.

For the steady-state solutions, a mesh of high resolution is desired. A high mesh resolution allows resolving small flow structures within the computational domain, as well as ensuring a good numerical accuracy. The highest volumetric cell density is found in the region near the turbulence inducing grid, to ensure the flow structure is resolved in its wake. In order to conserve cells, due to cell limitations and available computational time, high aspect ratio cells are used in the downstream region of the cathode channel, as well as the region between the inlet and turbulence inducing grid.

The structure of the mesh within the cathode flow channel and turbulence inducing grid for the steady state analysis can be seen in Fig. 2.10.

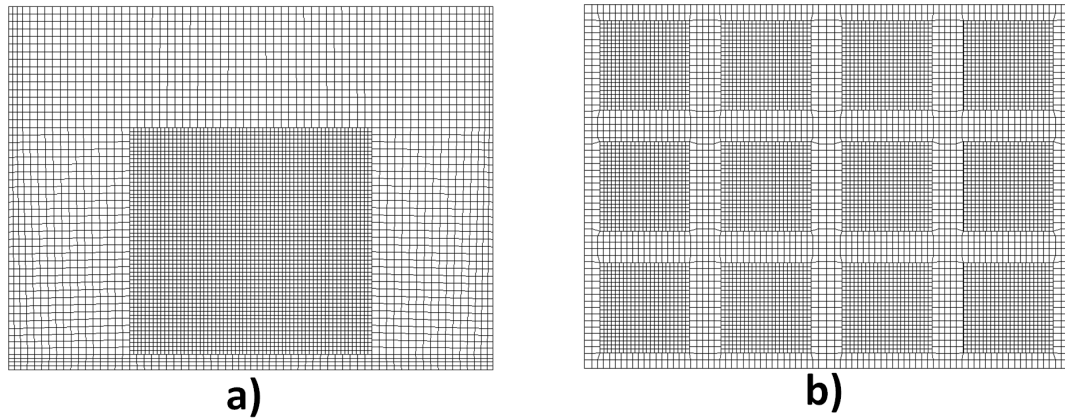


**Figure 2.10:** Structure of the mesh inside a) Cathode flow channel a) Turbulence inducing grid

Number of Cells	Max Skewness	Average Skewness	Maximum Aspect Ratio	Average Aspect Ratio	Cell Height (Viscous Region)
394,209	0.693	0.00187	253.19	14.883	0.04375 mm

**Table 2.4:** Mesh properties for steady-state analysis

In the transient analysis, unlike the steady-state, the solution field must be computed in each time step of the analysis. Using the method of calculating a time step shown in Eq. 2.35, a time step of 0.00004 sec is calculated. To achieve a 15 seconds flow time, it requires 375 000 time steps with multiple iterations each time-step. To do this with a mesh similar to the one in the steady-state analysis, several months of computational time would be needed with the available hardware. This would simply not be feasible within the allocated time frame. To reduce the computational time from months to days, a coarser mesh is used for the transient analysis.



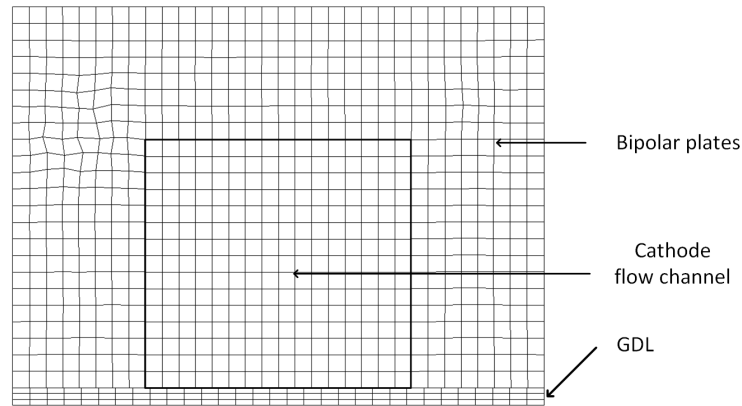


**Figure 2.11:** Structure of the mesh inside the cathode flow channel

A mesh region in the Z-Y plane used for the transient analysis is seen in Fig. 2.12.

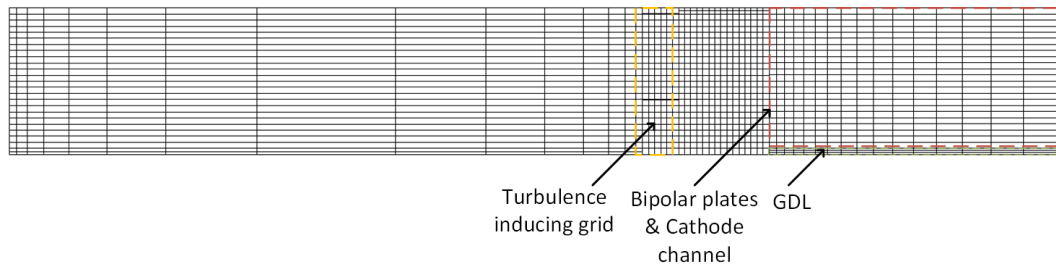


**Figure 2.12:** Mesh near turbulence grid region used in transient analysis

Number of Cells	Max Skewness	Average Skewness	Maximum Aspect Ratio	Average Aspect Ratio	Cell Height (Viscous Region)
59,837	0.8677	0.0442	122.29	9.1556	0.175 mm

**Table 2.5:** Mesh properties for transient analysis

## 2.2 Governing Equations and Models

In order to use Computational Fluid Dynamics, the equations that describe the fluid motion must be implemented in a correct manner. Which equations are chosen and how they are treated and solved will define the numerical method for the case.

Also, the conditions that validates the usage of certain equations must be fulfilled. Some of the most important conditions to consider, will be listed here:

- Lagrangian or Eulerian framework.

Lagrangian: Individual fluid elements are tracked through time and space. Meshfree method in a CFD case.

Eulerian: Fluid properties is a function of time and space  $\mathbf{u} = f(x, t)$ . Fixed mesh in a CFD case.

- Compressible or incompressible flow.

If the variation in density for a flow has a significant effect on the governing equation, it must be accounted for. A good rule of thumb is that if  $\mathbf{u}_{max} > \text{Mach } 0.3$  then the air is treated as compressible.

- Steady or unsteady flow.

If flow variables are time dependent, the flow is unsteady and a transient simulation must be performed. Otherwise, a steady-state solution can be found.

- Viscous or non-viscous.

If the stresses caused by the fluids viscosity has a significant influence on the solution, it must be accounted for. Otherwise it can be neglected.

- Turbulent or laminar flow.

The existence of turbulence within fluid flow has a significant impact on important parameters, such as fluid mixing, heat transfer, pressure loss etc. A compatible turbulence model must be used to account for these contributions. The existence of turbulence can be predicted by evaluating the local Reynolds number to the critical Reynolds number for the relevant flow scenario.

## 2.2.1 Governing Equations

The purpose of this report is to investigate the effect of a turbulence inducing grid on heat transfer, so energy must be accounted for in the governing equations. In Sec. 2.4, the velocity within the cathode channel was calculated to be 3.36 m/s, so, air incompressibility can be assumed. Furthermore, a Eulerian framework is used since there is only one fluid phase. Viscosity will be accounted for, although viscous heating as well as gravity forces will be neglected.

### Incompressible Navier-Stokes Equations

The equations describing the type of fluid flow mentioned above, is the incompressible Navier-Stokes equations. In conservation form, using Einstein notation, these equations are seen in Eq. 2.9 & 2.8 [7].

$$\text{Continuity:} \quad \frac{\partial u_i}{\partial x_i} = 0 \quad (2.8)$$

$$\text{Momentum:} \quad \rho \frac{\partial u_i}{\partial t} + \rho \frac{\partial}{\partial x_j} (u_j u_i) = -\frac{\partial p}{\partial x_i} + \frac{\partial}{\partial x_j} (2\mu s_{ij}) \quad (2.9)$$

$$(2.10)$$

Where,  $s_{ij}$  is the strain-rate tensor:

$$s_{ij} = \frac{1}{2} \left( \frac{\partial u_i}{\partial x_j} + \frac{\partial u_j}{\partial x_i} \right) \quad (2.11)$$

In steady-state solutions, there is no change in variables with respect to time so the term  $\rho \frac{\partial u_i}{\partial t}$  in the momentum equation will be equal to zero.

### Energy Equation

Since the CFD problem contains heating and cooling of the fuel cell channel, the energy equation in Eq. 2.12 is applied to both solid and fluid volumes.

$$\text{Energy:} \quad \rho C_p \left( \frac{\partial T}{\partial t} + (\mathbf{u} \cdot \nabla) T \right) = k_{eff} \nabla^2 T + S_E \quad (2.12)$$

Here, the variable  $k_{eff}$  denotes the effective conductivity of the material. For the fluid phase, this variable will be the sum of both air conductivity  $k$  as well as the additional conductivity due to turbulence  $k_t$ , which will be calculated based on the turbulence model implemented.

### Incompressible RANS Equations

The Reynolds-averaged Navier-Stokes (RANS) equations is the time-averaged equations of the Navier-Stokes equations describing fluid flow. In order to obtain the RANS equations, a Reynolds decomposition is performed.

The velocity and pressure term is decomposed into a mean and fluctuating part.

$$u_i = U_i + u'_i, \quad p = P + p' \quad (2.13)$$

Where, the mean and fluctuating velocities must satisfy:

$$\bar{u}_i = U_i, \quad \bar{u}'_i = 0 \quad (2.14)$$

$$\bar{p} = P, \quad \bar{p}' = 0 \quad (2.15)$$

Here, the overbar denotes that it is a time averaged value.

Using Eq. 2.13 in Eq. 2.8 & 2.9, the incompressible RANS equations are formulated:

$$\text{Continuity:} \quad \frac{\partial U_i}{\partial x_i} = 0 \quad (2.16)$$

$$\text{Momentum:} \quad \rho \frac{\partial U_i}{\partial t} + \rho \frac{\partial}{\partial x_j} (U_j U_i) = -\frac{\partial P}{\partial x_i} + \frac{\partial}{\partial x_j} (2\mu S_{ij} - \rho \overline{u'_i u'_j}) \quad (2.17)$$

$$(2.18)$$

Where,  $S_{ij}$  is the strain-rate tensor:

$$S_{ij} = \frac{1}{2} \left( \frac{\partial U_i}{\partial x_j} + \frac{\partial U_j}{\partial x_i} \right) \quad (2.19)$$

The  $-\rho \overline{u'_i u'_j}$  term on the right side of Eq. 2.17, is known as the Reynolds stress tensor, and contains six components in three dimensions. By decomposing the Navier-Stokes equations into the RANS equations, six additional unknown variables are introduced. Since no additional equations have been gained, the model is open and will need additional equations in order to become a closed set of equations. Several approaches to achieve this exist and is the turbulence model used to close the RANS equations. The approaches that will be used for this case, are introduced in the following section.

## 2.2.2 General Transport Equations

Looking at Eq. 2.8, 2.9 and 2.12 there is some obvious commonalities between the equations. If a general variable  $\phi$  is introduced to represent all scalar quantities such as velocity, temperature etc. A general transport equation can be written in the following form:

$$\frac{\partial \rho \phi}{\partial t} + \nabla \cdot (\rho \mathbf{u} \phi) = \nabla \cdot (\Gamma_\phi \nabla \phi) + S_\phi \quad (2.20)$$

$$\begin{array}{l} \text{Rate of} \\ \text{increase of } \phi \end{array} + \begin{array}{l} \text{Flow of } \phi \text{ out} \\ \text{of element} \end{array} = \begin{array}{l} \text{Increase of } \phi \\ \text{due to} \\ \text{diffusion} \end{array} + \begin{array}{l} \text{Increase of } \phi \\ \text{from sources} \end{array} \quad (2.21)$$

Where,  $\Gamma_\phi$  is the diffusion coefficient for  $\phi$ . Eq. 2.20 is the transport equation for  $\phi$  and clearly highlights the various transport processes within an arbitrary fluid or solid volume. This equation will need to be discretized with respect to both time and space, in accordance to the finite volume method.

### 2.2.3 Turbulence Modelling

The existence of turbulence for a fluid flow problem leads to complex interactions at a wide range of time and length scales due to turbulent eddies. These effects will need to be accounted for using a numerical method. The numerical methods used for this purpose can roughly be divided into three categories.

**RANS turbulence models:** By taking the time averaged solution of the Navier-Stokes equations, extra terms appear. These extra terms must be modelled using additional equations. Classical turbulence models typically used are the  $k$ - $\epsilon$ ,  $k$ - $\omega$  and Reynolds Stress Model (RSM). A comparison of RANS turbulence models is given in Tab. 2.6.

**Large Eddy Simulation:** Here the unsteady Navier-Stokes equations are space filtered so that larger eddies are resolved while rejecting smaller eddies. The unresolved small eddies are included using a sub-grid scale model. This method is more computationally demanding than RANS turbulence modelling since unsteady equations need to be computed.

**Direct numerical simulation:** This approach requires computing both mean as well as fluctuating flow velocity due to turbulence. Unsteady Navier-Stokes equations are solved with a mesh sufficiently fine to resolve even the smallest length scales. The time step also needs to be small enough to capture even the highest frequency fluctuations. This is the most computationally demanding approach that can be used.

A preliminary turbulence model study was conducted. The steady flow velocity and temperature field was compared using a variety of the turbulence models available in Ansys Fluent 19.2. The purpose of this study was to compare results between turbulence modelling methods and rule out any method that produces nonphysical or unrealistic results for this specific fluid flow problem.

In Fig. 2.13 velocity contours near the turbulence inducing grid and cathode channel inlet is seen for every turbulence modelling method investigated. The laminar results are used for comparison, since no turbulence modelling is used.

It should be mentioned that the  $k$ - $\epsilon$  model is the most widely used turbulence model for industrial applications. However,  $k$ - $\epsilon$  models perform best at high Reynolds number problems with fully turbulent flow structures. The local Reynolds numbers within the cathode channel is in the range of 100-400 dependent on the analysis. Therefore,  $k$ - $\epsilon$  is not well suited for this type of low Reynolds number study and is excluded from the preliminary study.

	Eddy viscosity:	Advantages:	Disadvantages:
<b>One equation models:</b>			
Spalart-Allmaras	$\mu_t = \rho \tilde{\nu} f_{v1}$	Very economical model with good accuracy for wall-bounded flows and with mild separation and recirculation	Developed for aerodynamic flows and not general industrial flows. Produces large errors in some free shear and jet flows.
<b>Two equation models:</b>			
k- $\epsilon$	$\mu_t = \rho C_\mu \frac{k^2}{\epsilon}$	Very robust model, most commonly used model for industrial flows. Good accuracy for a wide range of flows.	Inaccurate for many flows with strong streamline curvature, rotations and low Re numbers.
k- $\omega$	$\mu_t = \alpha^* \rho \frac{k}{\omega}$	Can accurately model the near wall region without modifications, better than k- $\epsilon$ for low Re flows.	Sensitive to boundary values of $\omega$ . Requires finer mesh near wall boundaries.
k- $\omega$ SST	$\mu_t = \rho \frac{k}{\omega}$	Uses a blending function to combine the advantage of k- $\epsilon$ in the outer layer and k- $\omega$ in the inner layer of wall. Not as sensitive to boundary values as k- $\omega$ . Considered the best RANS model for bounded aerodynamic flows and heat transfer prediction.	More difficult to converge than k- $\epsilon$ and k- $\omega$ .
<b>Seven equation models:</b>			
Reynolds Stress Model (RSM)	$\mu_t = 0.9 \frac{k^2}{\epsilon}$	Does not rely on isotropic turbulence assumptions. Each component of the Reynolds stresses have a transport equation. Considered the most general applicable turbulence model available.	Less economical. 50-60% more CPU time required per iteration and more iterations needed for convergence.

Table 2.6: Comparison of RANS turbulence models.

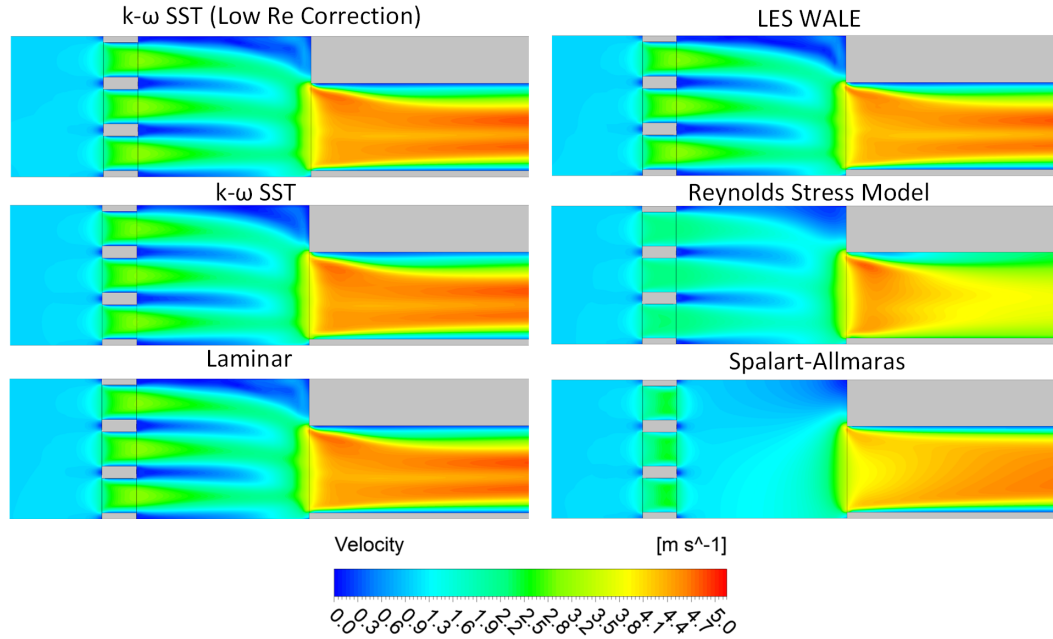


**Figure 2.13:** Velocity contour plots near turbulence inducing grid using different turbulence models

From Fig. 2.13 similarities are seen between the  $k-\omega$  SST, LES and Laminar velocity contours. In the Reynolds stress model, the expected near wall velocity gradient is not present in the turbulence inducing grid or the cathode channel. The Spalart-Allmaras model produces some obvious unrealistic flow structures downstream of the turbulence inducing grid.

Since heat transfer is the primary objective of this study, a directional temperature profile of the GDL can be seen in Fig. 2.14.

Fig. 2.14 also shows the Reynolds stress and Spalart-Allmaras model producing significantly different temperature profiles than the other models. Based on what is seen from both Fig. 2.13 & 2.14, the turbulence model that will be used for the steady state analysis is  $k-\omega$  SST and Large Eddy Simulation will be used for transient analysis, in order to resolve some of the larger eddy formations.

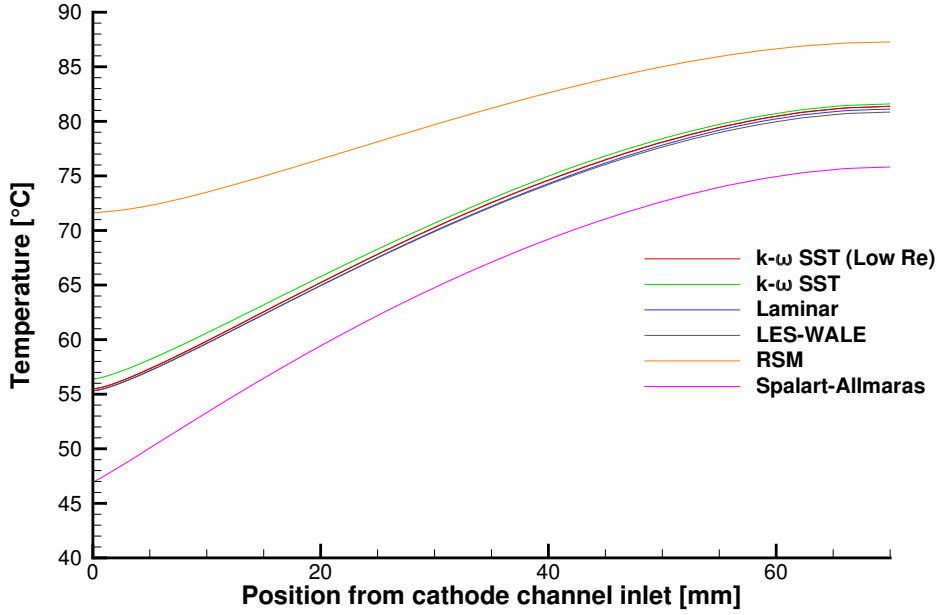


Figure 2.14: Directional GDL temperature plot using different turbulence models

### Bousinessq Approximation

Joseph Bousinessq proposed in 1877 that the Reynolds stress tensor  $\rho \overline{u'_i u'_j}$  is proportional to the mean rates of fluid deformation. This is expressed mathematically as: [12]

$$\tau_{ij} = -\rho \overline{u'_i u'_j} = \mu_t \left( \frac{\partial U_i}{\partial x_j} + \frac{\partial U_j}{\partial x_i} \right) - \frac{2}{3} \rho k \delta_{ij} \quad (2.22)$$

Where,  $k$  is the turbulent kinetic energy (TKE) equal to  $\frac{1}{2}(\overline{u'^2} + \overline{v'^2} + \overline{w'^2})$ ,  $\mu_t$  is the eddy or turbulent viscosity and  $\delta_{ij}$  is the Kronecker delta ( $\delta_{ij} = 1$  if  $i = j$  and  $\delta_{ij} = 0$  if  $i \neq j$ ).

A commonly used non-dimensional variable used to quantify the amount of turbulence is the turbulent viscosity ratio  $\mu_t/\mu$  which is simply the ratio between the turbulent viscosity calculated under Bousinessq approximation and the molecular dynamic viscosity of the fluid.

### k- $\omega$ SST

The k- $\omega$  Shear Stress Transport (SST) model was developed to combine the strength of the k- $\omega$  model in the near-wall region with the k- $\varepsilon$  in the turbulent far field re-



gion. To achieve this, both models are multiplied with a blending function and added together. This blending function is 1 in the near-wall region and activates the k- $\omega$  model, while approaching zero away from the walls. Furthermore, the turbulent or eddy viscosity is modified to account for any transport of any turbulent shear stress. The eddy viscosity is calculated as  $\mu_t = \frac{\rho k}{\omega}$  in the k- $\omega$  SST model.  $\omega$  here is the specific dissipation rate of turbulent kinetic energy (k).

The transport equations for k and  $\omega$  are seen in Eq. 2.23 & 2.24:

$$\rho \frac{\partial}{\partial t}(k) + \rho \frac{\partial}{\partial x_i}(k \cdot u_i) = \frac{\partial}{\partial x_j} \left( \Gamma_k \frac{\partial k}{\partial x_j} \right) + G_k - Y_k \quad (2.23)$$

$$\rho \frac{\partial}{\partial t}(\omega) + \rho \frac{\partial}{\partial x_i}(\omega \cdot u_i) = \frac{\partial}{\partial x_j} \left( \Gamma_\omega \frac{\partial \omega}{\partial x_j} \right) + G_\omega - Y_\omega + D_\omega \quad (2.24)$$

In these equations,  $G$  is the generation,  $Y$  the dissipation and  $\Gamma$  is the effective diffusivity of k or  $\omega$ .

### Large Eddy Simulation (LES)

In fluid flow problems where large eddies interact significantly with the mean flow, the Boussinesq Approximation is no longer valid due to the anisotropic nature of large eddy formation. The best option for such problems would be a Direct Numerical Solution (DNS) approach, where all length and timescales of turbulent eddies are resolved. However, due to the computational power this would require this is often not feasible. Large eddies are dependent on the flow and geometrical conditions, whereas small eddies are universal and mostly independent of flow or geometry. Therefore, large eddies are directly resolved, while small eddies and their effect on the large eddies are modeled using a sub-grid scale model.

In LES a spatial filter function  $G(\mathbf{x}, \mathbf{x}', \Delta)$  is applied to the unsteady Navier-Stokes equation in the defined domain:

$$\bar{\phi}(\mathbf{x}, t) = \int_{Domain} \phi(\mathbf{x}', t) G(\mathbf{x}, \mathbf{x}', \Delta) d\mathbf{x}' \quad (2.25)$$

Where,

$\bar{\phi}(\mathbf{x}, t)$  is the filtered function (overbar means spatial filtering not time averaging)

$\phi(\mathbf{x}', t)$  is the unfiltered function

The variable  $\Delta$  defines the filter cutoff width which can take any user defined value. However, when using the finite volume method, it does not make sense to choose a value smaller than the cell size used in the mesh, meaning that FVM applies an inherent filtering to the LES method. This inherent filtering due to cell size is commonly the only filtering method used, and is also what is used for this case.

## 2.3 Numerical Method

### 2.3.1 Spatial Discretization

The integral form of Eq. 2.20 for an arbitrary control volume is as follows:

$$\int_{CV} \frac{\partial \rho \phi}{\partial t} dV + \oint (\rho \mathbf{u} \phi) \cdot d\vec{A} = \oint (\Gamma_\phi \nabla \phi) \cdot d\vec{A} + \int_{CV} S_\phi dV \quad (2.26)$$

Eq. 2.26 is applied on each cell in the computational domain. An example cell is given below in Fig. 2.15. Cell discretization of Eq. 2.26 yields the following equation:

$$\frac{\partial \rho \phi}{\partial t} V + \sum_{N_{faces}} (\rho_f \mathbf{u}_f \phi_f) \cdot \vec{A}_f = \sum_{N_{faces}} (\Gamma_\phi \nabla \phi) \cdot \vec{A}_f + S_\phi V \quad (2.27)$$

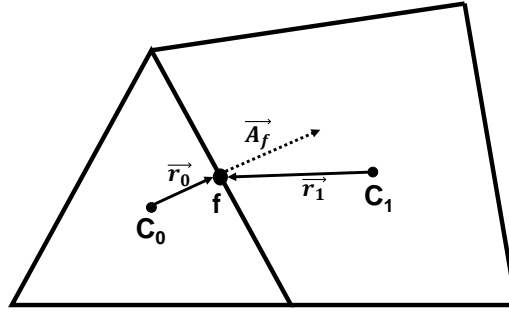


Figure 2.15: Control volume example for spatial discretization

$\phi$  is only calculated and stored at cell centers, but in Eq. 2.27 the value  $\phi_f$  is evaluated at the face and is required for the convection term. To evaluate these values, an interpolation scheme must be used. A computational cheap and common scheme to use is the first order upwind scheme, where  $\phi_f$  is simply equal to the cell center value upstream. For further numerical accuracy, the second order upwind scheme will be used. Face values are hence evaluated according to the expression in Eq. 2.28:

$$\phi_f = \phi + \nabla \phi \cdot \vec{r} \quad (2.28)$$

### 2.3.2 Temporal Discretization

During transient simulations, the general transport equation must be discretized in both space and time. The spatial discretization for transient simulations is identical

to what was described above, temporal discretization however requires integration of every term in the general transport equation over a time step  $\Delta t$ . The time evolution of  $\phi$  can be expressed:

$$\frac{\partial \phi}{\partial t} = F(\phi) \quad (2.29)$$

Where,  $F(\phi)$  is any spatial discretization as the one seen in Eq. 2.15. A first order implicit temporal discretization, using a simple backward difference approach, will then be expressed:

$$\frac{\phi^{n+1} - \phi^n}{\Delta t} = F(\phi^{n+1}) \quad (2.30)$$

For more numerical accuracy, a bounded second order implicit time integration will be used. "implicit" integration means that  $\phi^{n+1}$  in any given cell is related to  $\phi^{n+1}$  in neighboring cells through  $F(\phi^{n+1})$ . This allows for iteratively solving each time step, before moving on to the next. It also makes the solution unconditionally stable for any step size. The temporal discretization that will be used is expressed as:

$$\frac{\partial \phi}{\partial t} = \frac{\phi_{n+\frac{1}{2}} - \phi_{n-\frac{1}{2}}}{dt} \quad (2.31)$$

$$\phi_{n+\frac{1}{2}} = \phi_n + \frac{1}{2}\beta_{n+\frac{1}{2}}(\phi_n - \phi_{n-1}) \quad (2.32)$$

$$\phi_{n-\frac{1}{2}} = \phi_{n-1} + \frac{1}{2}\beta_{n-\frac{1}{2}}(\phi_{n-1} - \phi_{n-2}) \quad (2.33)$$

Where,  $\beta$  is a bounding factor at that time level for turbulent flow parameters i.e. turbulence kinetic energy, dissipation rate and specific dissipation rate.

### Calculation of time step

As mentioned above, when using implicit time integration, the solution is unconditionally stable for all time steps. However, in order to get realistic results, there are some good practices to follow. It is important that the temporal resolution matches or exceeds the spatial resolution. Based on the Courant–Friedrichs–Lewy or CFL condition, this statement can be expressed: [5]

$$\Delta t \leq \frac{\Delta x}{U} \quad (2.34)$$

Where,  $\Delta x$  is the largest edge length of a cell and  $U$  is the local average velocity. To account for deviations from the average velocity, a good approximation for  $\Delta t$ ,

which will be used to calculate the time step, will be:

$$\Delta t \approx \frac{\Delta x}{2U} \quad (2.35)$$

The quite strict restriction on the time step in Eq. 2.35 is only required for LES. Unsteady RANS equations have different time step requirements. However, only transient LES will be performed in this report so this restriction will be applied to calculate the time step.

### 2.3.3 Solution Algorithm

In Sec. 2.2.1 the incompressible Navier-Stokes equation were introduced, and in three dimensions they would yield four equations with four unknowns  $u, v, w$  and  $p$ . Intuitively this should be an easy set of equations to solve. However only equations for  $u, v, w$  exists since the continuity equations is more a restriction on the momentum equation than an equation that can be solved. To overcome this problem, a solution algorithm can be used which has the following two key functions:

1. Derive an equation for the pressure  $p$  from the momentum and continuity equations.
2. Make a corrector for the velocity field, in order to satisfy the continuity equation.

Several popular algorithms exist such as SIMPLE, SIMPLEC, PISO and COUPLED, which each have their own advantages and disadvantages dependent on the application. For this study, the ANSYS Fluent default solver will be used, which is the SIMPLE algorithm.

#### SIMPLE Algorithm

SIMPLE or Semi-Implicit Method is an iterative solving algorithm used for pressure-velocity coupling. Essentially, it functions as a guess and correct procedure for pressure calculations. The full explanation and derivation of the processes used in the SIMPLE process will not be presented in this report, but the general idea of the algorithm is seen in Fig. 2.16.

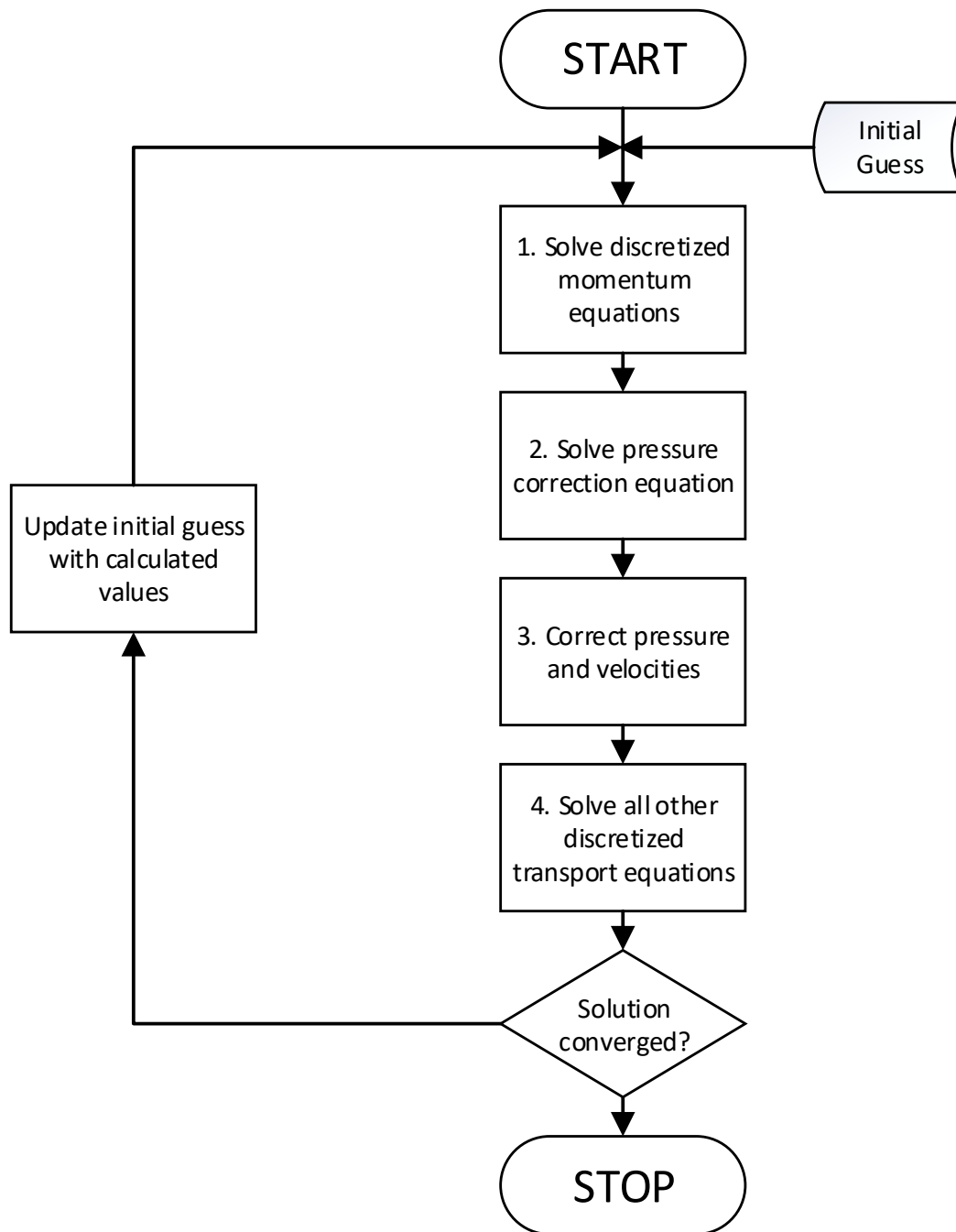


**Figure 2.16:** Flowchart of the SIMPLE algorithm used



## Chapter 3

# Results and Discussion

In this chapter the results from the conducted CFD studies will be presented and discussed. The presentation of results will be divided into two main sections, steady-state results in Sec. 3.1 and transient results in Sec. 3.2. Due to limited amount of computational time available, the same mesh could not be used for the transient simulations as for the steady-state, so a direct comparison between steady-state and transient solutions will not be performed.

Results will be presented using three key parameters: velocity, temperature and turbulence intensity. The turbulence intensity is the fraction of the velocity fluctuations with respect to a reference velocity, and is a common way of normalizing the turbulence level into a non-dimensional parameter. Turbulence intensity is defined as:

$$I = \frac{u'_i}{U_{ref}} \quad (3.1)$$

Where,  $u'_i$  is the root mean square of the velocity fluctuations and  $U_{ref}$  is a reference velocity set in the ANSYS Fluent reference values task page. This value was left unaltered at its default value of 1 m/s. When performing a steady-state analysis,  $u'_i$  can be estimated from the turbulent kinetic energy  $k$  in the following manner:

$$u'_i = \sqrt{\frac{1}{3}(u'^2_x + u'^2_y + u'^2_z)} = \sqrt{\frac{2}{3}k} \quad (3.2)$$

Combining Eq. 3.1 & 3.2, we get the expression for turbulence intensity used in the calculations that will be presented:

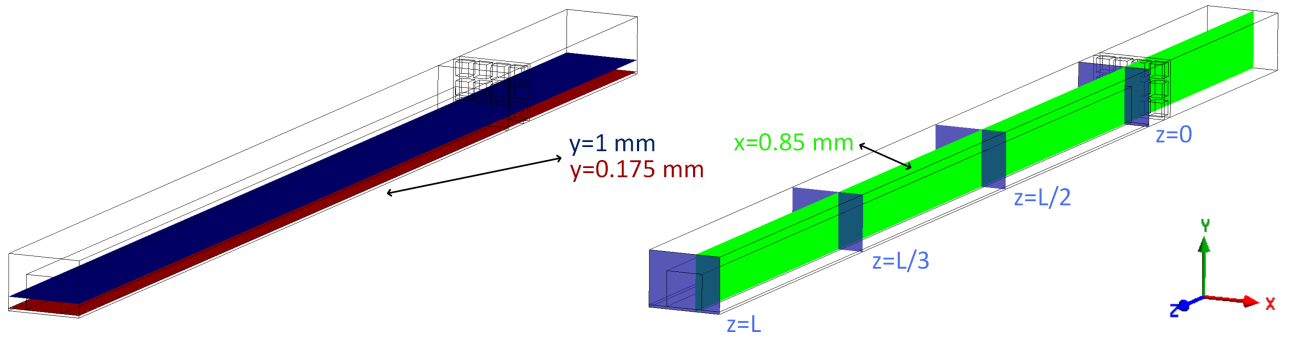
$$I = \frac{\sqrt{\frac{2}{3}k}}{U_{ref}} = \frac{\sqrt{\frac{2}{3}k}}{1 \text{ m/s}} \quad (3.3)$$

### 3.1 Steady-state

Steady-state results were obtained in order to determine the effectiveness of a turbulence inducing grid and its location in relation to the inlet of the cathode flow channel. The mesh, boundary conditions and method used for the analysis was presented in Ch. 2. A tight convergence criterion was used, meaning that the variation for all residuals was below  $10^{-4}$  before calculations were stopped.

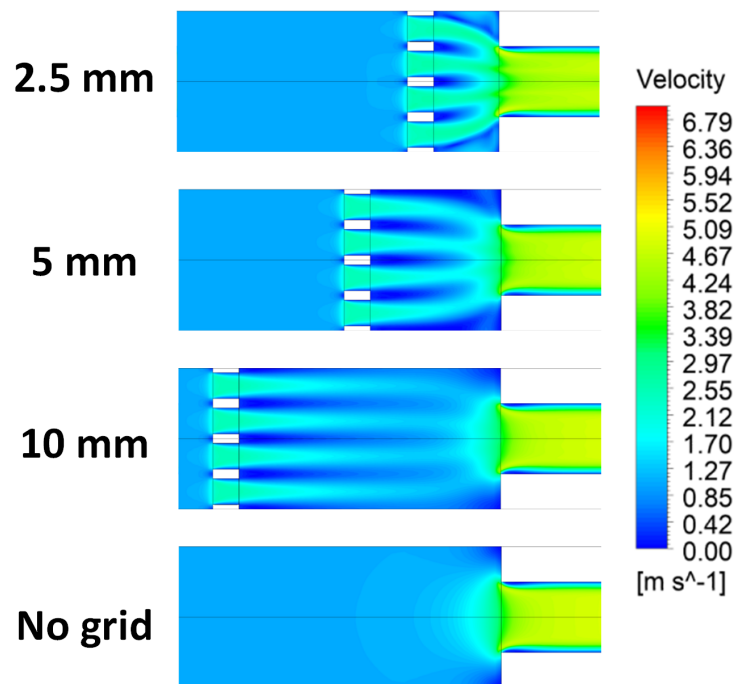
#### 3.1.1 Effect of Turbulence Inducing Grid and Its Location

To evaluate the effect of the turbulence inducing grid and its distance from the cathode flow channel, contours are shown in the planes seen in Fig. 3.1. Additionally, XY-plots are shown to better evaluate the directional development of important variables within the cathode flow channel.



**Figure 3.1:** Location of contour planes in the computational domain



**Contours in the Z-X plane**

**Figure 3.2:** Velocity contours in the Z-X plane in fluid domain ( $y=1$  mm)

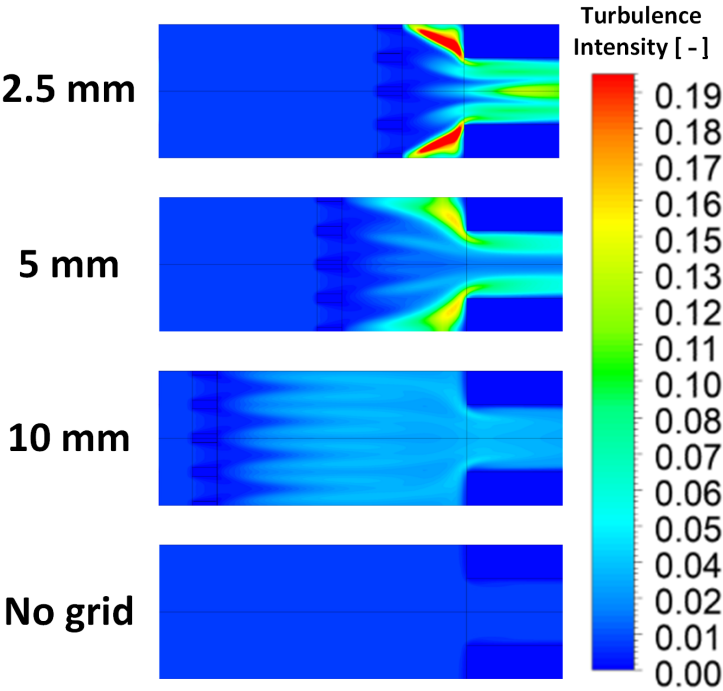


Figure 3.3: Turbulence intensity contours in the Z-X plane in fluid domain ( $y=1$  mm)

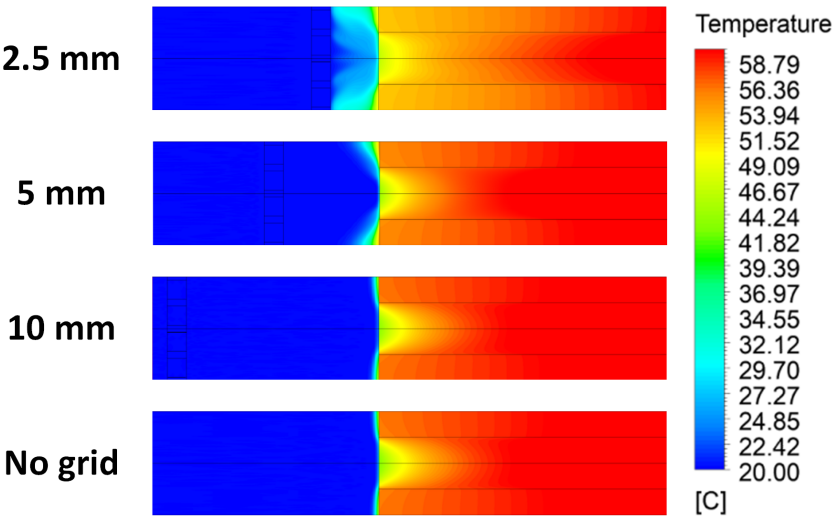


Figure 3.4: Temperature contours in the Z-X plane at GDL solid-fluid interface ( $y=0.175$  mm)

Contours in the Z-Y plane

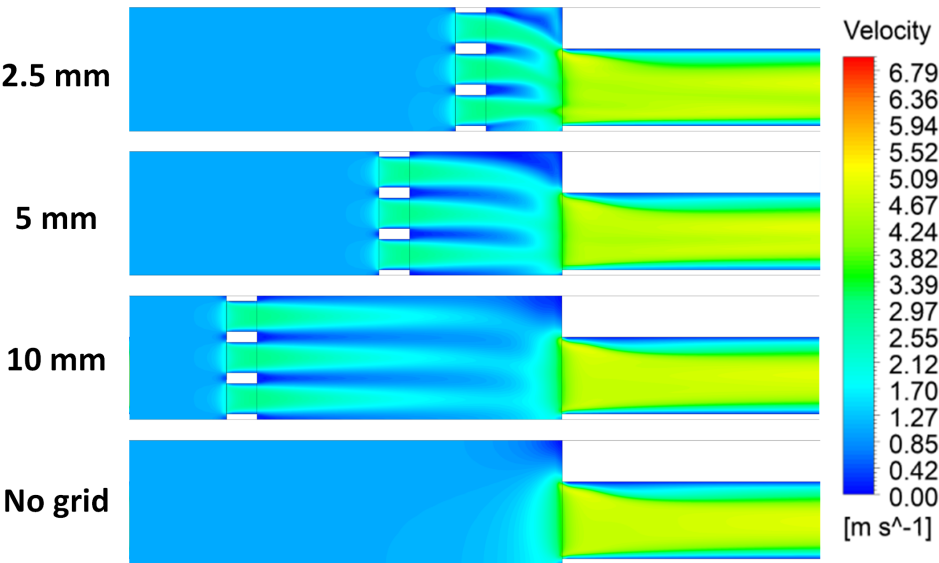


Figure 3.5: Velocity contours in the Z-Y plane ( $x=0.85$  mm)

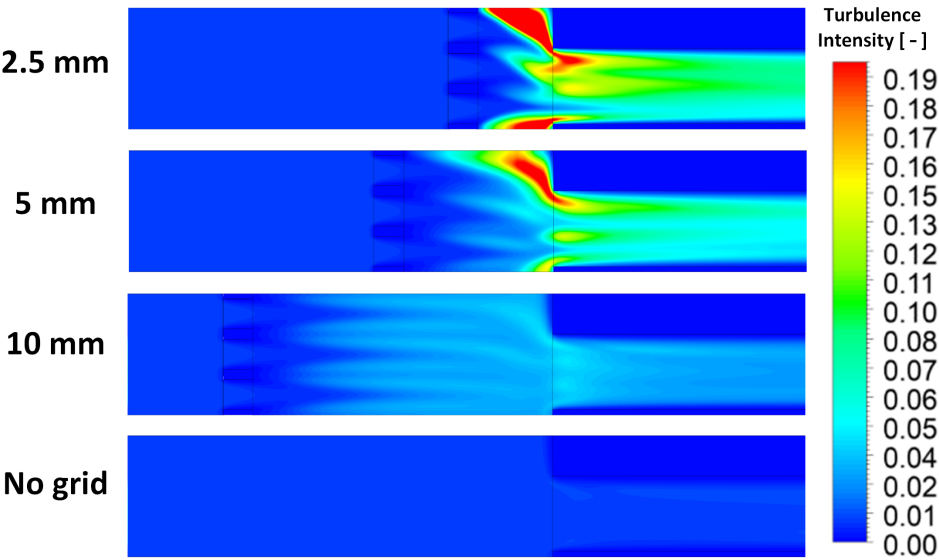


Figure 3.6: Turbulence intensity contours in the Z-Y plane ( $x=0.85$  mm)

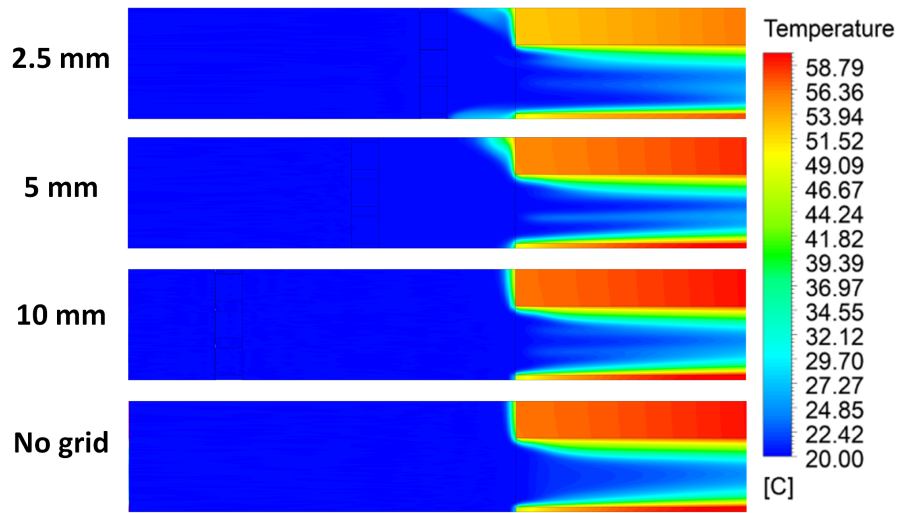


Figure 3.7: Temperature contours in the Z-Y plane ( $x=0.85$  mm)

#### Contours in the X-Y plane

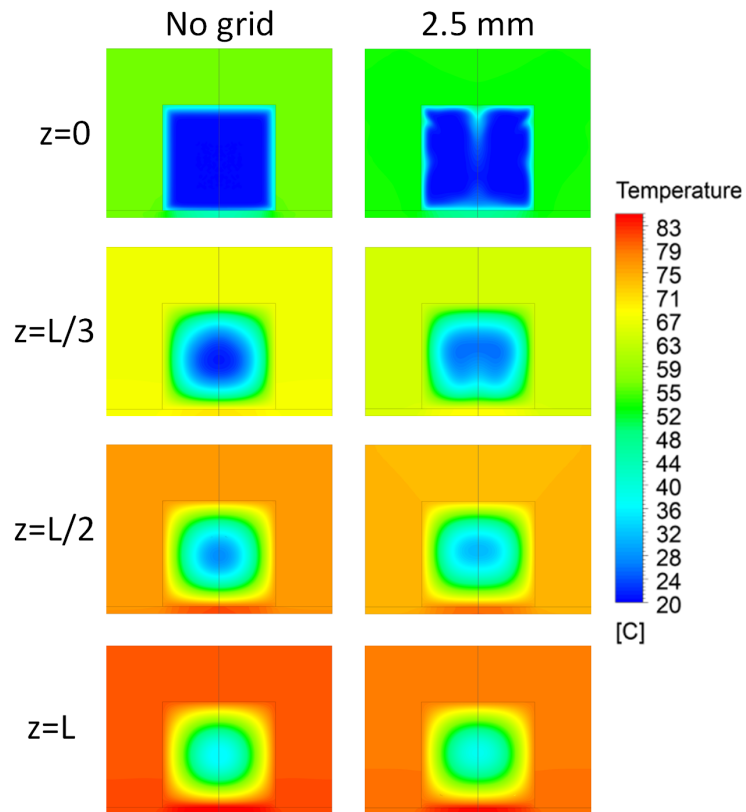
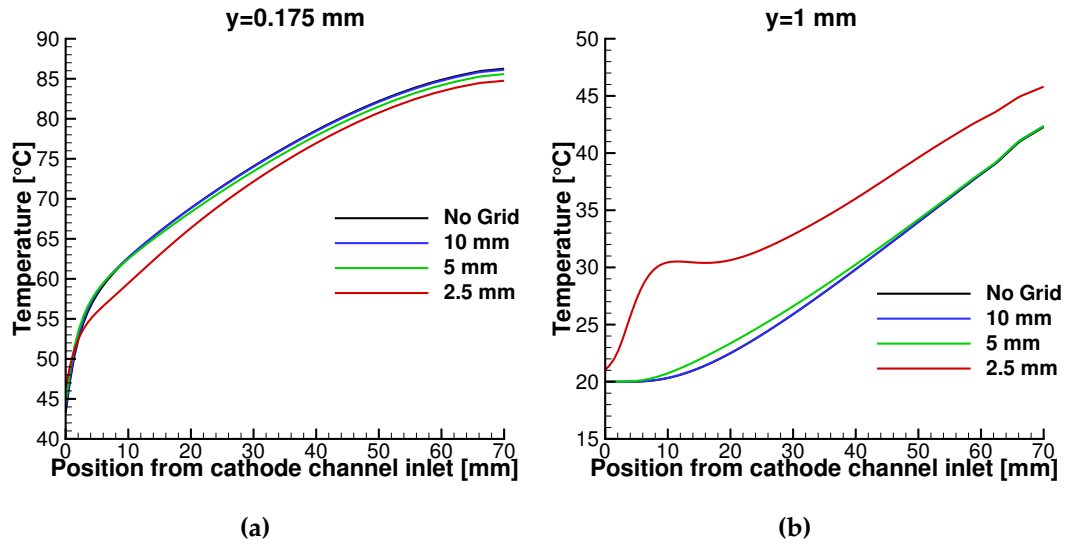
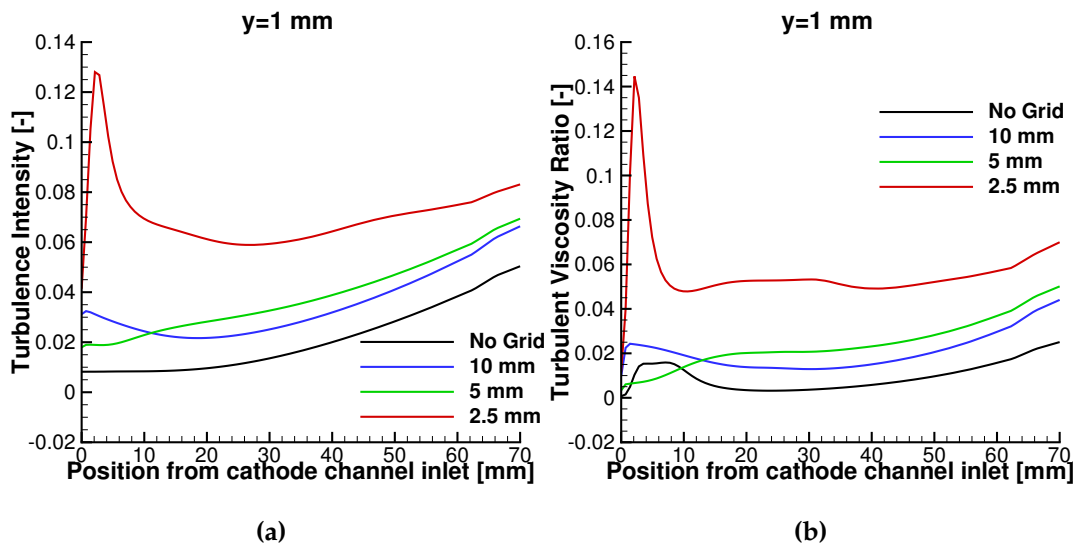


Figure 3.8: Temperature contours in the X-Y plane along the length of the cathode channel ( $L=70$  mm)

## X-Y Plots



**Figure 3.9:** Development of temperature along the symmetry plane in cathode channel for a) GDL b) Air



**Figure 3.10:** Development of turbulence intensity and turbulent viscosity ratio at  $y=1$  mm along the symmetry plane in cathode channel

### 3.1.2 Results Summary

The effect of the turbulence inducing grid is clearly seen as an uneven velocity distribution in the wake of the grid which produces turbulent kinetic. This results in a better heat conduction away from the solid surfaces, which lowers the temperature of the solid while increasing the air temperature. The lower temperature in the cathode channel entrance region is clearly seen in Fig. 3.4 & 3.7.

The temperature profile for both solid and air is better seen in Fig. 3.8 where a cross-section in the X-Y plane of the cathode flow channel is shown at various length of the channel for the no grid base case and with a 2.5 mm distance turbulence inducing grid. It is clearly seen that the temperature gradient of air is reduced by the grid until around halfway into the cathode flow channel ( $z=L/2$ ). The basic relation for heat transfer by convection is:  $\dot{Q} = hA\Delta T$  where  $h$  is the convective heat transfer coefficient,  $A$  is the surface area and  $\Delta T$  is the temperature difference between the wall and the air layer adjacent to the wall. The turbulence inducing grid is expected to increase both the convective heat transfer coefficient as well as the temperature difference due to increased fluid mixing in the cathode channel.

To summarize the results using some key variables, the maximum and average temperature measured in the computational domain is presented in Tab. 3.1.

	Maximum temperature (Solid) [°C]	Average temperature (Solid) [°C]	Pressure loss [Pa]	Relative difference from No Grid case
No Grid	86.42	71.06	38.13	0.00% / 0.00% / 0.00%
10 mm	86.29	71.08	41.24	-0.15% / +0.03% / +8.16%
5 mm	85.75	70.43	41.22	-0.77% / -0.88% / +8.12%
2.5 mm	84.90	68.53	42.00	-1.75% / -3.57% / +10.14%

**Table 3.1:** Steady state results

From Tab. 3.1 both the maximum and average temperature decreases when a turbulence inducing grid is used. However, a pressure loss of around 3 to 4 Pa is seen for all cases with a grid. The effectiveness of the grid with a 10 mm distance between the grid and cathode channel inlet is very low since only a negligible decrease in temperature is seen while still increasing the pressure loss. The 2.5 and 5 mm distances lowers the average operating temperature by around 2.5°C and 0.5°C respectively.

In conclusion a turbulence inducing grid, located 2.5 mm away from the cathode flow channel produced the most significant decrease on operating temperature of around 2.5°C at an increased pressure loss of around 4 Pa.

## 3.2 Transient

Based on the results from Sec. 3.1 a measurable difference in operating temperature was seen between the no grid and 2.5 mm case. In this section, these two cases will be compared in transient operation. A total of 15s flow time was calculated, and was initiated from a steady-state solution using the  $k-\omega$  SST turbulence model. The mesh used for the transient simulation is significantly coarser than what was used for the steady-state solution, in order to achieve a feasible computational time since 375000 time steps was needed (See Sec. 2.1.3).

The reasoning behind the transient study is to investigate the hypothesis that a fluctuating velocity profile within the cathode channel will lower the thermal resistance between the wall and fluid, which has been observed in other studies. Two sinusoidal velocity profiles is used as the inlet boundary conditions and calculated for both no grid and 2.5 mm cases. Both profiles has a period of 10s but with varying amplitudes (See Fig. 3.11).

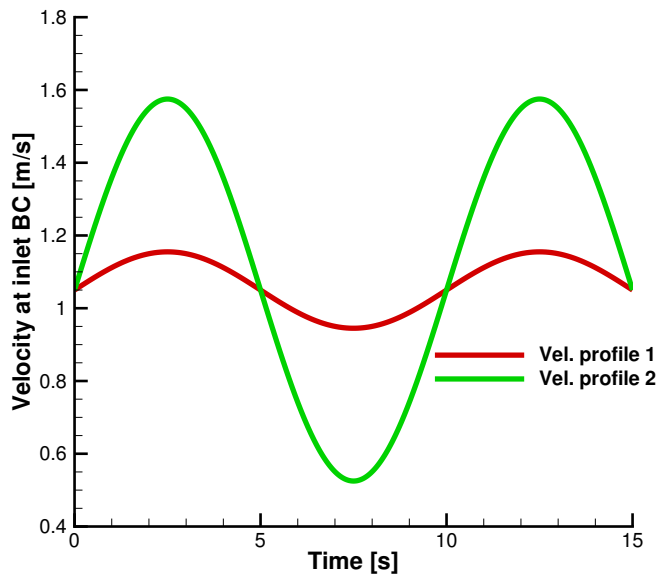
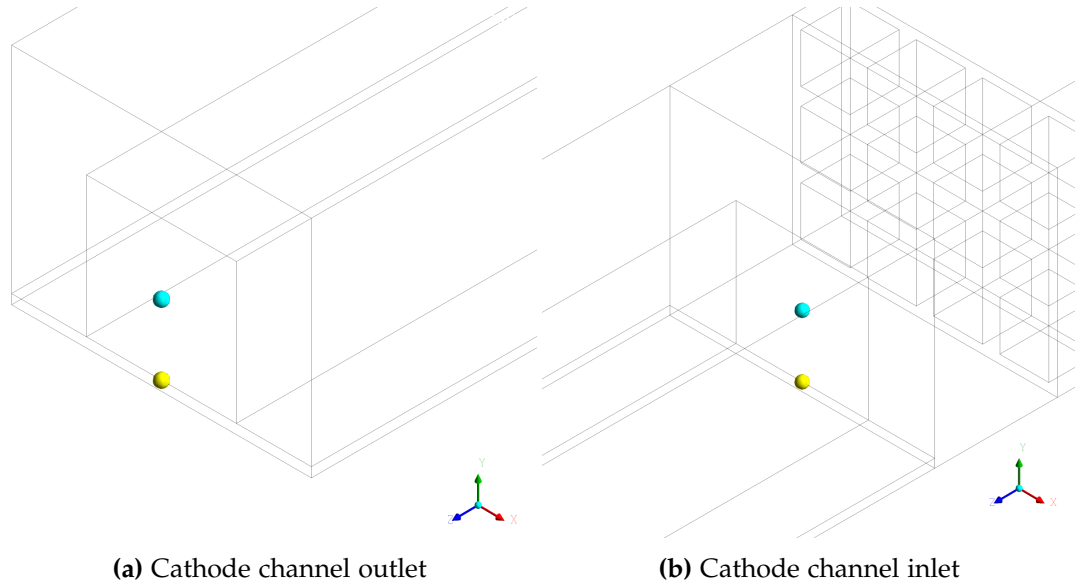


Figure 3.11: Velocity profiles used for the transient analysis

Time dependent velocity and temperature contours will be presented, as well as time series data from points at the inlet and outlet of the cathode channel. The locations where data will be obtained is seen in Fig. 3.12.



**Figure 3.12:** Locations where transient time series data will be evaluated

Four points are seen in Fig. 3.12, two at the cathode channel inlet and outlet. The point marked with a yellow ball is placed at a height of 0.175 mm, which means it will measure variables at the solid interface between the GDL and fluid domain. The cyan ball is placed at a height of 1.4375 mm, placing it in the geometric center of the cathode flow channel in the fluid domain. These four points should give an accurate representation on the effect on both the entrance and outlet region of the cathode channel. Intuitively, it is expected that the highest temperatures will be at the outlet region since fluid will be gradually heated as it passes through the cathode channel, reducing the temperature difference and by extension the convective heat transfer from solid to fluid.

Results from the transient analysis are presented below.



### 3.2.1 Effect of Time Dependent Velocity Inlet Under Transient Operating Conditions

Time dependent velocity contours

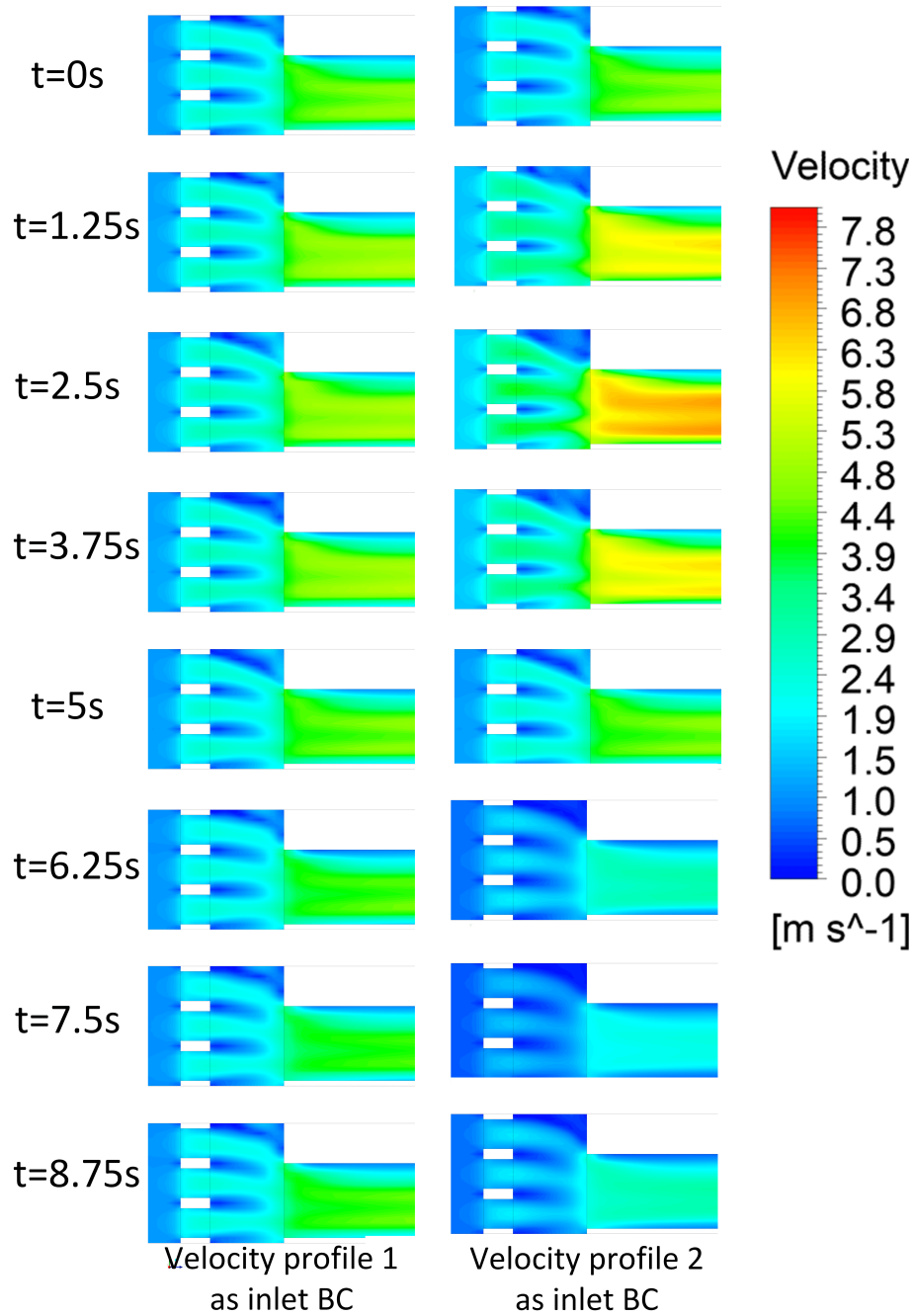
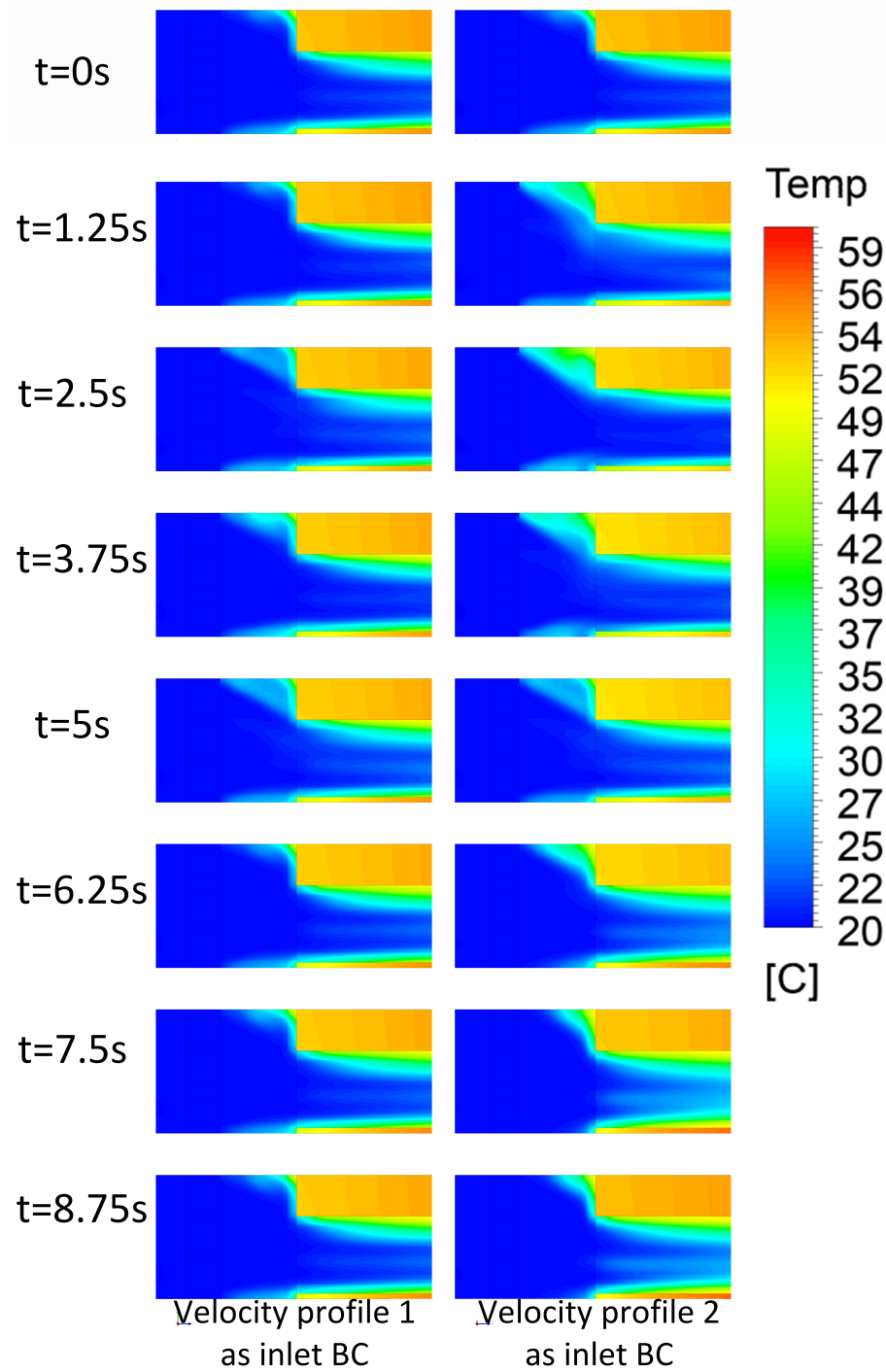


Figure 3.13: Velocity contours near the cathode channel inlet in the Y-Z plane at  $x=0.85$  mm

## Time dependent temperature contours



**Figure 3.14:** Temperature contours near the cathode channel inlet in the Y-Z plane at  $x=0.85$  mm

### Temperature time series at Cathode Channel Inlet

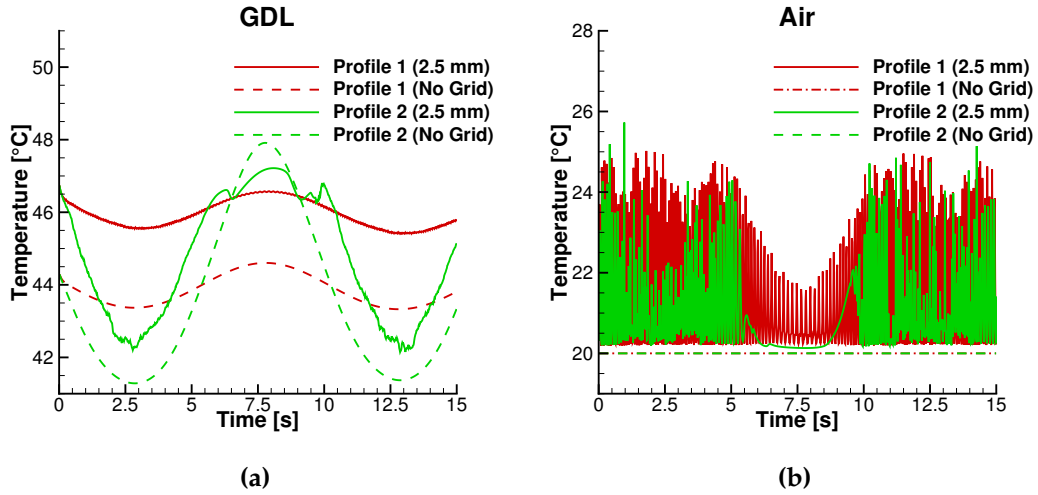


Figure 3.15: Temperature time series at cathode channel inlet for a) GDL b) Air

### Temperature time series at Cathode Channel Outlet

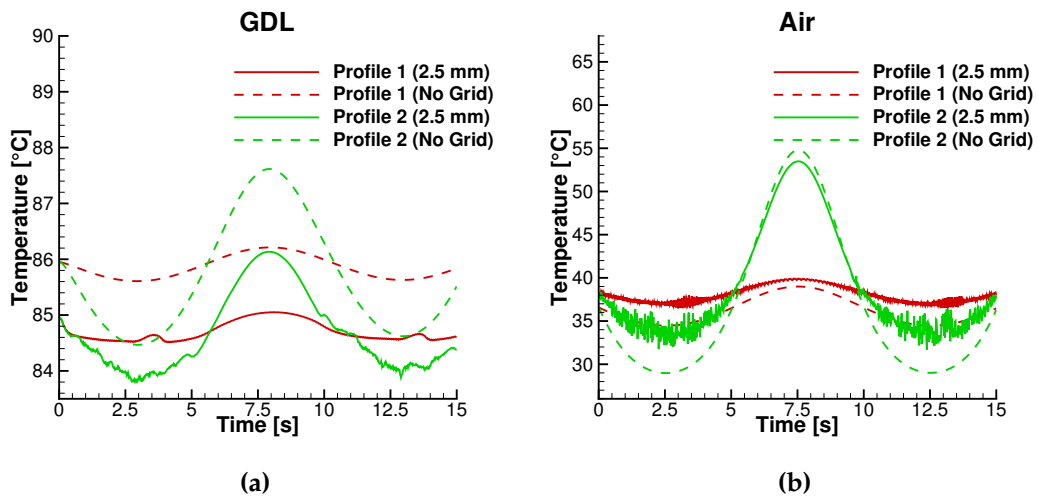


Figure 3.16: Temperature time series at cathode channel outlet for a) GDL b) Air

### 3.2.2 Results summary

In the transient analysis two cases with two unique velocity profiles were simulated with a flow-time of 15s. In Fig. 3.13 & 3.14 the changing velocity and temperature

is seen at different times of the simulation. At 2.5s the velocity is at its highest and should result in the lowest temperatures, which is seen for both velocity profiles but more pronounced for velocity profile 2. The effect of the fluctuating velocity profiles is better seen in the time-series plots of Fig. 3.15 & 3.16. The effect of the grid is clearly seen in Fig. 3.9b where the temperature fluctuates significantly when a grid is used due to rapid mixing in the entrance region of the cathode channel. For the no grid case, the temperature is constant at 20°C since no fluid mixing has occurred at that point. In general, temporal temperature fluctuations are much higher when a grid is used compared to the no grid case.

At the inlet of the cathode channel, the time averaged temperature of the GDL is 2°C lower than the steady-state solution when using velocity profile 2. At the outlet this effect is not as strong, and the time averaged temperature is only 0.3°C lower. In Tab. 3.2 the maximum, minimum and time averaged temperature of the GDL at both inlet and outlet are listed for both velocity profiles, as well as the steady state temperatures.

	Maximum temperature (GDL) [°C]	Minimum temperature (GDL) [°C]	Time-averaged temperature (GDL) [°C]	Steady-state temperature (GDL) [°C]
<b>Inlet</b>				46.74
Vel. Profile 1	46.74	45.4	45.39	
Vel. Profile 2	47.22	42.15	44.71	
<b>Outlet</b>				84.94
Vel. Profile 1	85.05	84.51	84.7	
Vel. Profile 2	86.13	83.8	84.66	

**Table 3.2:** Maximum, minimum and time averaged temperature of the GDL at the inlet and outlet of the cathode channel

In conclusion, the effect of a fluctuating velocity profile has an impact on the average operating temperature of the fuel cell channel. Based on the results seen in Tab. 3.2, velocity profile 2 outperforms velocity profile 1 in terms of lowering the time-averaged temperatures. A decrease of 2°C is seen at the inlet and 0.3°C at the outlet.

## Chapter 4

# Conclusion and Future Work

### 4.1 Conclusion

This thesis is about the cooling strategy feasibility of using a turbulence inducing grid on an air-cooled PEM fuel cell stack. Heat is released because of the irreversible polarization losses and internal resistances in the fuel cell stack. Using the known polarization curve of a fuel cell stack, the heat flux during operation at a current density of  $0.4 \text{ A/cm}^2$  was calculated to be  $2587 \text{ W/m}^2$ . This release of heat increases the temperature of the membrane electrode assembly (MEA) and bipolar plates, resulting in a loss of energy efficiency and the deterioration of fuel cell materials.

In an air-cooled PEM fuel cell, heat is removed by air in the cathode flow channel. The airflow inside the channel is usually laminar in nature with a Reynolds number in the range of 100-400. It is well known in fluid mechanics that the convective heat transfer is increased when the fluid is in a turbulent state, due to the presence of eddies which increases mixing and by extension heat and mass transfer. Previous experiments have shown that a turbulence inducing grid, could increase the power density of a fuel cell stack by over 30% as a direct consequence of the increased convective heat transfer.

A CFD study was conducted to see if the increase in heat transfer seen in experiments could be replicated numerically. Results showed that the average temperature of the Gas Diffusion Layer (GDL) inside the MEA, and the bipolar plates could be reduced by  $2.5^\circ\text{C}$  by installing a turbulence inducing grid at a distance of 2.5 mm from the cathode channel inlet. However, a additional pressure loss of approximately 4 Pa is added to the system, which is a relative pressure increase of 10% compared to not using a grid. It was also investigated whether a fluctuating velocity profile, would further reduce the thermal resistance between the cathode channel walls and air and result in a lower operating temperature. Results showed a further reduction of  $2^\circ\text{C}$  in the time-averaged temperature of the GDL near the

entrance region of the cathode channel and  $0.3^{\circ}\text{C}$  at the outlet, when compared to the steady-state solution. A sinusoidal wave velocity profile with a mean value of  $1.05\text{ m/s}$  with a  $\pm 50\%$  amplitude and a period of 10 seconds was used as the inlet boundary condition to achieve this reduction in operating temperature.

## 4.2 Future Work

Based on lessons learned from this thesis, the following points could be incorporated into any future work dealing with a similar problem:

- Heat flux as a function of average temperature in the solid domain could be used as a user defined boundary condition for transient simulations. A function for this relationship would need to be developed.
- Periodic boundary conditions could be applied to better model the stacked nature of fuel cell channels.
- Anode flow channel could be added to the computational domain using, since this also functions as a heat sink for the fuel cell channel. However, there is only a low flow rate of hydrogen compared to air at a stoichiometry of 50, so it would be a minimal effect.
- If an entire fuel cell stack is modelled, the convective and radiating heat transfer to the surroundings should be modelled. This would result in higher temperatures in the center of the stack.
- The GDL could be more accurately modelled as an an-isotropic porous media.
- Contact resistances between the GDL and bipolar plates should be modelled.
- If computational time and hardware allows, a more refined mesh should be used for transient simulation.
- An experiment could be performed in order to calculate the amount of turbulent kinetic energy in the wake of a turbulence inducing grid. This would help verify and calibrate the CFD model.
- The Reynolds Stress Model of turbulence, showed the largest differences in temperature between a grid and no grid. The model was deemed inaccurate for this case due to the appearance of unrealistic flow structures near wall boundaries. More time could have been used in examining this turbulence models validity for the flow problem. The Stress- $\omega$  version is probably the best candidate for this type of flow.

# Bibliography

- [1] Frano Barbir. "Chapter Four - Main Cell Components, Material Properties, and Processes". In: *PEM Fuel Cells (Second Edition)*. Ed. by Frano Barbir. Second Edition. Boston: Academic Press, 2013, pp. 73 –117. ISBN: 978-0-12-387710-9. DOI: <https://doi.org/10.1016/B978-0-12-387710-9.00004-7>. URL: <http://www.sciencedirect.com/science/article/pii/B9780123877109000047>.
- [2] Torsten Berning and Søren Knudsen Kær. "thermodynamic analysis of air-cooled proton exchange membrane fuel cells operated in different climate regions". In: *Submitted to ENERGY* (2019).
- [3] Torsten Berning, Saher Al Shakhshir, and Xin Gao. "The effect of a turbulence grid placed in front of the cathode inlet of an air cooled proton exchange membrane fuel cell". In: Unpublished. International Conference on Applied Energy. Västerås, Sweden, Aug. 2019.
- [4] Rasheed Fallah and Line Justesen Pløger. "Improving the performance of an air-cooled fuel cell stack by a turbulence inducing grid". MA thesis. Aalborg University, June 2018.
- [5] Ansys Inc. *Lecture 4: Large Eddy Simulation (LES) and Other Scale Resolving Simulation (SRS) Models*. Fluent V. 15.0 Lecture Series. 2014.
- [6] N. P. Mikhailova, E. U. Repik, and Yu. P. Sosedko. "Reynolds Number Effect on the Grid Turbulence Degeneration Law". In: *Fluid Dynamics* 40.5 (2005), pp. 714–725. ISSN: 1573-8507. DOI: 10.1007/s10697-005-0109-1. URL: <https://doi.org/10.1007/s10697-005-0109-1>.
- [7] Cuong Tan Nguyen. "Turbulence Modeling Cuong Nguyen November 05 , 2005 1 Incompressible Case 1 . 1 Reynolds-averaged Navier-Stokes equations". In: 2005.
- [8] P.E. Roach. "The generation of nearly isotropic turbulence by means of grids". In: *International Journal of Heat and Fluid Flow* 8.2 (1987), pp. 82 –92. ISSN: 0142-727X. DOI: [https://doi.org/10.1016/0142-727X\(87\)90001-4](https://doi.org/10.1016/0142-727X(87)90001-4). URL: <http://www.sciencedirect.com/science/article/pii/0142727X87900014>.

- [9] Ideen Sadrehaghighi. *Mesh Generation in CFD*. Apr. 2019. doi: 10.13140/RG.2.2.26522.54721/2.
- [10] Setareh Shahsavari et al. "Thermal analysis of air-cooled PEM fuel cells". In: *International Journal of Hydrogen Energy* 37.23 (2012), pp. 18261 –18271. ISSN: 0360-3199. DOI: <https://doi.org/10.1016/j.ijhydene.2012.09.075>. URL: <http://www.sciencedirect.com/science/article/pii/S0360319912021131>.
- [11] Toray. *Toray Carbon Fiber Paper "TGP-H"*. <http://www.fuelcellsetc.com/store/DS/Toray-Paper-TGP-H-Datasheet.pdf>.
- [12] H.K. Versteeg and W. Malalasekera. *An Introduction to Computational Fluid Dynamics: The Finite Volume Method*. Pearson Education Limited, 2007. ISBN: 9780131274983. URL: <https://books.google.dk/books?id=RvBZ-UMpGzIC>.